



Maya Vase Rollout Photography's Past, Present, and Potential in a Cross-Discipline Digital Future: A Proof-of-Concept Study

Citation

Reddick, Sandra. 2024. Maya Vase Rollout Photography's Past, Present, and Potential in a Cross-Discipline Digital Future: A Proof-of-Concept Study. Master's thesis, Harvard University Division of Continuing Education.

Permanent link

<https://nrs.harvard.edu/URN-3:HUL.INSTREPOS:37378375>

Terms of Use

This article was downloaded from Harvard University's DASH repository, and is made available under the terms and conditions applicable to Other Posted Material, as set forth at <http://nrs.harvard.edu/urn-3:HUL.InstRepos:dash.current.terms-of-use#LAA>

Share Your Story

The Harvard community has made this article openly available.
Please share how this access benefits you. [Submit a story](#).

[Accessibility](#)

Maya Vase Rollout Photography's Past, Present, and Potential in a Cross-Discipline Digital Future:

A Proof-of-Concept Study

Sandra Reddick

A Thesis in the Field of Anthropology and Archaeology
for the Degree of Master of Liberal Arts in Extension Studies

Harvard University

May 2024

Abstract

Vase rollout photography has emerged as an invaluable tool for artifact study and documentation, offering scholars a comprehensive, 360-degree perspective of an object's painted imagery and hieroglyphic texts. Over the past five decades, the creation of vase rollout images has predominantly relied on film and a specialized workstation pioneered by photographer and Mayanist Justin Kerr. The transition to modern digital methods has been gradual, characterized by limited and predominantly manual efforts. This thesis investigates the historical trajectory, current status, and potential future of digital vase rollout photography within the realm of archaeological documentation and study.

This thesis hypothesizes that recent advancements in digital photography coupled with image-processing and image understanding techniques from the field of computer vision can be integrated to automate the process of creating rollouts. The research and results presented here demonstrate that automated digital rollout images can be created with high quality and fidelity, suitable for use as a new standard form of artifact archival documentation. Through a novel combination of commercial off-the-shelf hardware and purpose built software, this thesis introduces a proof-of-concept experiment showcasing the attainability of excellent quality software-generated digital rollouts in a platform that requires minimal investment. The digital rollout archive made possible by this method is envisioned as a potentially valuable resource, supplying the necessary digital inputs for the creation of yet-to-be-developed artifact analysis tools in the future.

Frontispiece



**Image by Sandi Reddick. Digital photographic rollout of a reproduction of the Altar de Sacrificios vase (reproduction of K3120). The vase was purchased from acclaimed artist Patricia Martin Morales at her workshop in Muna, Mexico. The set of digital still images captured from this reproduction vessel provided the source inputs for much of the algorithm development, testing, and refinement that made this project possible. It was also the target of the first successful rollout using RedCarpet software. At the time this reproduction was purchased, I was unaware that a rollout of the original of this exquisitely painted Maya vessel was one of two rollouts that appeared in print in 1975, the first photographic rollouts of Maya vases ever published.*

Author's Biographical Sketch

Sandra Reddick is a candidate for the Master of Liberal Arts in Extension Studies at Harvard University, concentrating in Anthropology and Archaeology. Sandra holds Bachelor of Science in Computer Science from the University of Central Florida where she worked under a National Science Foundation REU (Research Experience for Undergraduates) grant implementing computer algorithms to detect symmetry in digital images. She went on to work in the image processing field on development of the FBI's AFIS (Automated Fingerprint Identification System) at Lockheed Martin Information Systems. Sandra has worked in both software and database engineering for over three decades.

In 2005, she met her husband, Gregory Reddick, also a software engineer. A long-time Mayanist and author of the Xoc Maya Calendar program, Gregory introduced Sandra to the field of Maya studies. They have been attending Mesoamerican conferences together since 2006 (he since 1994) and they have traveled extensively in the Maya regions of Mexico, Guatemala, Belize, and Honduras.

Sandra resides in the Pacific Northwest with her husband and their Golden Retriever, Ella. All three enjoy spending time together sailing in the Salish Sea on their thirty-two foot sailboat, *Achernar*.

Dedication

To Justin Kerr, whose stunning portfolio of Maya vase rollouts, and selfless sharing of his work, knowledge, and time kindled my interest in Maya vases and lit the spark that led me towards this effort.

To my mom, who ignited my love of travel and made my first visit to the Maya ruins at Tulum possible, beginning my lifelong fascination with the Maya and other historical cultures. I know you would have been so incredibly proud. You are always missed and never forgotten.

To my husband Greg, the love of my life and partner in every adventure. Your unwavering belief in my capabilities has been the driving force behind the completion of this thesis. Your constant support has made this scholarly endeavor not just mine but ours.

Acknowledgments

The completion of this work would never have been possible without the support and guidance from many of whom each made my experience at Harvard truly unforgettable. First and foremost, my thanks go to Dr. John R. Stilgoe to whom I am deeply grateful for his consistently supportive and uplifting guidance as thesis director. My profound thanks go to Dr. Richard Martin for counseling me throughout the thesis proposal phase and for being a key mentor since the beginning of my Harvard journey. I appreciate the excellent advice you've given me at every decision point, and it has been an honor and privilege to have had the opportunity to learn from you.

I also want to express my sincere thanks to Emily Pierce Rose, Academic Outreach Coordinator, whose tireless assistance made it possible to complete this project using artifacts from the Peabody Museum's Pre-Columbian art collections. Your support in curating artifacts, scheduling viewing rooms, and handling artifacts during photography was critical to this project's success, and for that, I'm immensely grateful.

My deepest appreciation goes to Dr. Jennifer Loughmiller-Cardinal, scholar, mentor, and friend. Your steadfast support, consistent encouragement, and insightful feedback over the past four years have been instrumental in improving my writing competence significantly, for which I am profoundly grateful.

My thanks also go to Alexandre Tokovinine and Julie Hoggarth who, in addition to Jennifer Loughmiller-Cardinal, kindly consented to interviews in support of this project.

I also want to extend my deep gratitude to Joshua Cook, my Director of Engineering. As a part time graduate student with a full-time career in technology, this academic journey would not have been possible without your gracious flexibility and trust in me to balance work and school effectively.

Finally, to my amazing husband, Gregory Reddick: without you, this thesis would never have been written. Your belief in me and pride in my accomplishments have been a constant source of motivation throughout this multi-year academic journey and I'm eternally grateful.

Table of Contents

Frontispiece.....	iv
Author’s Biographical Sketch.....	v
Dedication.....	vi
Acknowledgments.....	vii
List of Tables	xii
List of Figures	xiii
Chapter I. Introduction.....	1
Chapter II. Review of the Literature	4
Early Rollouts in Archaeological Study	4
Justin Kerr’s Contribution.....	6
A Short History of Peripheral Photography.....	8
Maya Vase Rollouts in Print.....	9
Photogrammetry and Digital Scanning Methods.....	12
Making the Case for Rollouts	14
The Future of Rollouts in the Digital Era	15
Chapter III. Materials and Methodology	16
Hardware – The Workstation.....	19
The Camera Setup.....	20
Lighting.....	21
Turntable	23

Miscellaneous Hardware.....	24
Software – Red Carpet.....	25
Background.....	25
Image Capture.....	27
Image Pre-Processing.....	28
Rollout Construction.....	29
Proof of Concept.....	30
Process Overview.....	31
Phase One: Image Capture.....	32
Phase Two: Image Pre-processing.....	34
Phase Three: Rollout Creation.....	37
Chapter IV Results and Analysis.....	38
Quality Scoring Methodology.....	38
Subjective Scoring Results.....	41
Distortion.....	41
Ghosting.....	42
Shear.....	46
Objective Scoring Review.....	50
Combined Scoring and Review.....	55
Chapter V. Conclusions.....	59
Limitations.....	59
Next Steps.....	60
Appendix 1. Rollout images.....	62

Appendix 2. Rollout Workstation Components, Costs, and Sources	77
Appendix 3. MATLAB Code Used in Objective Quality Analysis.....	79
Appendix 4. SSIM Results.....	88
References.....	94

List of Tables

Table 1.	Artifact selection with difficulty categorization and rationale	17
Table 2.	Subjective Quality Scoring	39
Table 3.	Subjective evaluation scores	49
Table 4.	Structural Similarity (SSIM) Score.....	52
Table 5.	Artifact distortion, ghosting, shear, and SSIM evaluation results	57
Table 6.	Workstation Hardware	77

List of Figures

Figure 1.	Hand-drawn rollout example.	5
Figure 2.	Composite (mosaic) photographic rollout example.	6
Figure 3.	Composite (mosaic) photographic rollout example.	11
Figure 4.	Workstation Setup.....	33
Figure 5.	R23007 distortion example.	42
Figure 6.	R23003 ghosting example.....	43
Figure 7.	R23009 ghosting example.....	44
Figure 8.	R23010 distortion, ghosting, and shear example.	45
Figure 9.	R23007 shear example.....	47
Figure 10.	R23014 shear example.....	48
Figure 11.	R23006 SSIM maximum (excellent match) example.	53
Figure 12.	R23007 SSIM minimum (poor match) example.....	54

Chapter I.

Introduction

In the study of Mesoamerican art and epigraphy, vase rollout photography proves an instrumental tool in both the study and documentation of artifacts. It provides scholars with a comprehensive, 360-degree view of an object's painted images and hieroglyphic texts. Prior to the development of the rollout image, only a portion of a cylindrical surface and its details were observable at one time. This photographic technique enables scholars to view an entire scene from a cylindrical vessel in one image.

This thesis presents the results of research into the past, present, and potential future of digital vase rollout photography and its role in archaeological documentation and study. Chapter 2 examines the historical evolution of rollout methodologies in the documentation and publication of Mesoamerican vases. This review looks at the diverse techniques used to create rollouts, including hand-drawn rollouts, mosaics created using still photographs, and film-based rollout photographs. The chapter discusses the scholarly use of rollout images and highlights the advantages of this method of artifact archival documentation. Additionally, an in-depth review of emerging digital photographic techniques in artifact documentation and analysis within the discipline offers insights into both the manual methodologies being employed and the current limitations inherent in the creation of digital vase rollouts.

This thesis hypothesizes that current advancements in both digital photography and image-processing algorithms can now be integrated within purpose-built software to capture high-quality photographic images in order to automate the creation of vase and

other artifact rollouts. More broadly, this thesis aims to prove that software-generated digital rollout images can be created with sufficient fidelity across a range of vessel forms and artifact types which are suitable for use in a variety of academic contexts, including as a new standard form of artifact archival documentation. To test this hypothesis, a proof-of-concept experiment was conducted using a low-cost, low barrier-to-entry rollout photography workstation paired with domain-specific custom developed rollout software. This experiment leverages available image processing (manipulation) and image understanding (knowledge extraction) algorithms in a novel combination to achieve quality automated rollout image creation. Chapter 3 details the equipment, software, and methods used within the execution of this proof-of-concept experiment, while Chapter 4 presents the methods and rationale for evaluating the resulting rollout images.

With an automated documentation platform available to researchers, universities, museums, and other institutions, digital rollout photography has the potential to extend its application beyond the narrow domain of Maya vase studies. Modest investment requirements make this platform viable for broader integration into diverse archaeological contexts. Many different archaeological contexts provide examples where photographic rollouts could prove useful. Like their Maya counterparts, Greek urns often contain imagery whose study could benefit from a single 360-degree view provided by a rollout. Delicately carved cylinder seals are found in a variety of ancient cultures, including Mesoamerica, Egypt, Sumeria, Mesopotamia, and others. For these fragile objects, the use of a digital rollout photography workstation may provide a preferable method for documentation. In contrast to the conventional technique of seal rolling in putty or clay, the platform demonstrated here offers a non-invasive means for 360-degree

image capture and rollout creation. Rollout photography can play a crucial role in supporting archival initiatives and enhancing scholarly study while safeguarding fragile artifacts from potential damage. Furthermore, the versatility of such workstations extends to the potential incorporation of multi-spectral imaging techniques, enhancing the depth and breadth of artifact analysis in a non-intrusive manner.

Archival documentation of decorated vessels using a robust, automated, and high-quality digital photography platform has the potential to do more than just replace its older analog counterpart in the field of Maya vase studies. A new digital rollout archive with even minimal image-understanding algorithms applied can be leveraged as inputs into entirely new image analysis and pattern matching algorithms which have yet to be developed. Such algorithms have the potential to assist archaeologists with analysis, provide a means for digital cataloging, and eventually perform automated identification of related imagery and common hieroglyphic components within a new form of digital imagery database. Beyond the needs of scholars today, it can also provide a critical digital documentation platform for more advanced computational analysis of these artifacts into the future.

Chapter II.

Review of the Literature

Scholars who study Maya vases have turned to rollout images for over a century to provide them with an all-in-one view of their highly artistic scenes and hieroglyphic texts. Although there is ample evidence within Maya studies literature to suggest that rollout images play an important role in the documentation and study of Maya vases, there is scant mention of the contribution these rollout images provide to archaeological study. There is also little discussion of the methods of creating such images. The perceived value and importance of rollouts in archaeological study appear to be commonly accepted. Modern advancements in digital image capture and image processing technologies have been revolutionizing the field of photography. However, adoption and incorporation of these advancements into the field of Maya vase studies, specifically with respect to the creation of vase rollouts from digital still images, has been limited.

Early Rollouts in Archaeological Study

The earliest studies and scholarly publications which examined Maya art included rollouts of polychrome vessels (Spinden 1913; Rands 1974; Coe 1975). Rollout images quickly became an important tool scholars used, shared, and published as the study of Maya art and epigraphy advanced. Prior to the availability of high-quality analog rollout

photographs, hand drawn (see Figure 1) or painted rollout images were created for archival documentation and publication (Spinden 1913; Coe 1975).

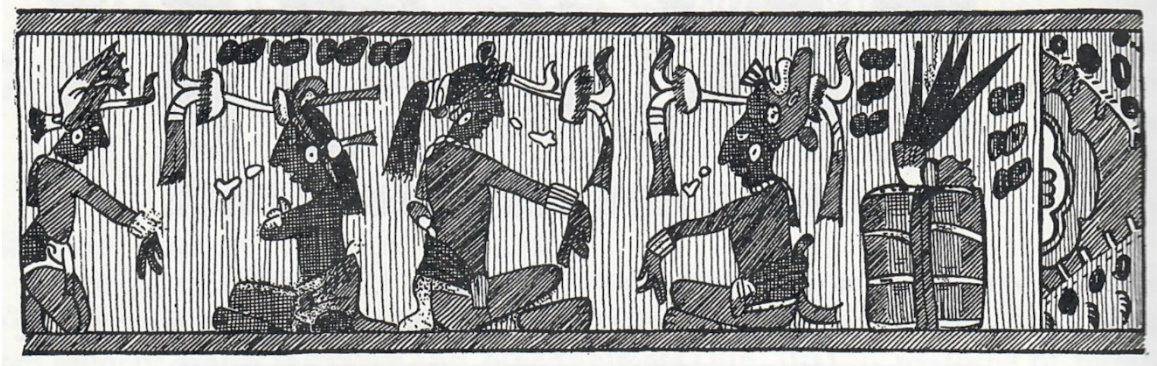


Figure 1. Hand-drawn rollout example.

This hand-drawn rollout from 1913 is of the same Maya vessel included in this project identified as R23006 (see rollout images in Appendix 1). This single 360-degree rollout was included in Herbert J. Spinden's 1913 publication of "A Study of Maya Art: Its Subject Matter and Historical Development", based on his 1909 Harvard University PhD thesis.

Some of the earliest examples of composite rollouts appeared in a 1940s publication titled *The Maya and Their Neighbors* (Hay et al. 1940, plates VI, VIII). Also called mosaic images, these early photographic rollouts were constructed by hand from a series of still film-based images. Individual images were carefully cut and laid side-by-side to match up their edges to provide a contiguous 360-degree photographic view of the vessels for the reader. Although rudimentary and sometimes distorted or flawed, they demonstrate an early desire for a single contiguous view of the vessels (see Figure 2).



Figure 2. Composite (mosaic) photographic rollout example.

This composite rollout was created by Justin Kerr and accessed online from the Maya Vase Database. Designated K114, it is one of the earliest photographic composite rollouts Kerr created.

By the 1970s, many scholarly publications in the field of Maya studies routinely included hand drawn or photographic composite rollouts of Maya vases. Despite the availability of rollout photography, drawn renderings continue to be used within many scholarly publications (Tokovinine 2013b; Stone and Zender 2011; Fash 2001). This may be attributable, at least in part, to the high cost, limited availability, numerous technical limitations, or simply the difficulty of creating high quality rollout photographs.

Justin Kerr's Contribution

While the inclusion of the first Maya vase rollouts in scholarly publication goes back over a century to Herbert J. Spinden's seminal work, *A Study of Maya Art* (1913), scholars attribute the adoption of vase rollout photography within the field of Maya studies to Justin Kerr (Doyle 2016). Kerr pioneered the creation of a peripheral

photography camera in the 1970s in a studio he dedicated to photographing Maya vases (B. Kerr and Kerr 2005). The majority of Maya vase rollout photographs since that time were produced by him. Kerr's six volumes of *The Maya Vase Book: A Corpus of Rollout Photographs of Maya Vases* (J. Kerr et al. 1989; 1990; 1992; 1994; 1997; 2000) constitutes a masterpiece collection of his rollout photography. In conjunction with the online Maya Vase Database, Kerr's influence in the adoption of rollout photography is recognized as a valuable tool in the study of Maya vases (J. Kerr, n.d.; Reents-Budet 1994).

In examining Kerr's contribution to Maya vase studies with his rollout photographs, relatively few mentions of the role these photographs play in scholarly study have been made in print beyond providing image credits. However, recognition for this important tool isn't entirely missing. In *Painting the Maya Universe: Royal Ceramics of the Classic Period*, Reents-Budet acknowledges Kerr and his rollouts, stating: "Justin's amazing rollout photographs allow us to see and study the compositional and epigraphic features of Classic Maya painted pottery. Without these rollout views....this book could not hope to be a lasting contribution..." (1994, xviii). Similarly in an article published in the journal *Ancient Mesoamerica*, Loughmiller-Cardinal notes that these rollout photographs "...provide an essential tool for analyzing vessel scenes. However, the flat representations should not be used at the expense of appreciating and studying the scribal use of the curved surface." (writing as Loughmiller-Newman 2008, 39). Loughmiller-Cardinal explained that the fact that this needed to be mentioned, that there are reasons to continue study using the original artifacts and not just Kerr's rollouts, demonstrates clearly what a significant and valuable tool these rollouts have become within the field of

Maya vase studies (Jennifer Loughmiller-Cardinal, e-mail message to author, September 1, 2023).

Yet despite being well over a century since the first rollout sketches appeared in publication, hand-drawn images of these vessels still routinely appear in scholarly publication (Fash 2001; Miller and Brittenham 2013; Stone and Zender 2011; D. Stuart 2011). This is not surprising considering sketches are still easier and less costly to create than images produced by Kerr's unique custom-built rollout camera. As film photography becomes less prominent in comparison to digital alternatives, scholars must investigate the advantages and drawbacks of digital photography, particularly within the evolving domain of computational photography. This exploration is essential for transitioning Maya vase rollout photography and photographic archival practices for Maya vases into the digital era.

A Short History of Peripheral Photography

While Kerr's development of an analog (film) rollout photography platform in the late 1970s was a valuable contribution to the field of Maya studies, other peripheral cameras used to create rollout photographs were already established, although expensive and not widely available. In 1967, a rollout photograph of a standard automobile engine piston appeared in a photography exhibition in New York titled *Once Invisible* (Museum of Modern Art [MoMA] 1967). The exhibition's press release described the photographs as "wondrous and beautiful images that exist in the world but cannot be seen by the human eye without the aid of photography" (Museum of Modern Art [MoMA] 1967).

In 1971, Andrew Davidhazy's experimental rollout peripheral photography, abstract human faces and bodies, was published on the cover of the Sunday supplement, *Milwaukee Journal Insight* (Lockwood and Davidhazy 1971). Lockwood described Davidhazy's slit-scan camera, and noted how distortion could be introduced when the speed of the moving film did not exactly match the rotation of the camera's subject. Precise synchronization between the film's movement and the subject is needed to achieve archival-quality rollout images for artifact documentation using this method.

Maya Vase Rollouts in Print

Kerr created his first Maya vase rollouts for Michael Coe's *The Maya Scribe and His World* (1973). These rollouts were not created using rollout photography, but rather the published images were painted by artists based on a series of Kerr's adjacent still photographs (J. Kerr 2007). Two rollout photographs of Maya vases appeared in print for the first time in the December 1975 *National Geographic* issue on the Maya. These images were created by the well-known *National Geographic* photographer Otis Imboden. The article "Riddle of the Glyphs" described the process used to create rollout photographs with a purpose-built slit scan camera (G. E. Stuart 1975). A diagram of the camera and turntable were also included to explain this unconventional photographic process in the popular monthly magazine. Kerr's (2007) *A Short History of Rollout Photography* mentions that this *National Geographic* issue was published at the same time as he was experimenting with rollout photography for photographing Maya vases. Kerr describes his early attempts at creating rollouts and building a rollout workstation using a Hasselblad camera body, a phonograph turntable, belts, and a coffee can as his subject.

Kerr's first Maya vase rollout photographs subsequently appeared in print in 1978's *Lords of the Underworld* (Coe and Kerr 1978; J. Kerr 2007). Although not the first rollout photographs to appear in print, Kerr's rollout photographs quickly became the standard in this field. Kerr continued to create rollout photographs of Maya vessels for nearly fifty years with his last "new" images created in 2016 (Justin Kerr, email message to author, January 30, 2019). Each object in this database has been assigned a unique K, or Kerr, number to identify it. Kerr's extensive photographic collection of nearly 2000 Maya vessels is freely available for study online through the Maya Vase Database Project (J. Kerr, n.d.).

Kerr's rollouts appeared prominently within Robicsek's definitive work titled *The Maya Book of the Dead: The Ceramic Codex; The Corpus of Codex Style Ceramics of the Late Classic Period* (1981). Containing upwards of 200 vessel rollouts, this comprehensive examination could not have been presented satisfactorily without Kerr's body of work. Yet, about these rollouts, the volume simply states that "All rollout photographs were taken by Mr. Justin Kerr..." (Robicsek 1981, xvi). Robicsek also notes that where rollout photographs were not available, true for many of the vessels presented in the study, he assembled composite rollout images (see Figure 3) and comments on them, stating that "the proportions may be somewhat distorted owing to the convexity of the objects depicted" (1981, xvi). He later explains: "By including such (composite) photographs in this study, we have compromised to some degree the appearance of our book rather than relented our effort to present the reader with a comprehensive survey of the material." (Robicsek 1981, xvi). Here the author makes his case for why it is

preferable to include lesser quality rollouts than to have no rollout for presentation within his discussion.



Figure 3. Composite (mosaic) photographic rollout example.

This composite rollout was created by Francis Robicsek for inclusion in “The Maya Book of the Dead: The Ceramic Codex; The Corpus of Codex Style Ceramics of the Late Classic Period” (Robicsek 1981). It demonstrates a desire to include rollouts in the discussion, even when a quality rollout photograph does not exist for an object.

The Kerr collection includes one manually constructed rollout from digital stills, image K9317, added in 2017. The stitching distortions created at each transition are clearly present in the final rollout image. A similar manually constructed digital image, hand-stitched by Kerr using Photoshop, also appears in a 2019 Sotheby’s publication (Justin Kerr, email communication to author, May 1, 2019; “Maya Polychrome Cylinder

Vase Late Classic, Circa AD 550-950” 2019). These appear to be the only two digital photographic composite rollout images pieced together by Justin Kerr prior to his retirement in 2019. The overall difficulty of producing a quality rollout with the labor-intensive preparation of images suitable for stitching has severely limited the adoption of creating such rollouts.

One notable Maya vase rollout image appears in the book *Road to Ruins* (Graham 2010, 446–47). Ian Graham includes one photographic rollout image in this volume with the caption: “My roll-out photo of the British Museum’s “Fenton Vase” (taken around 1966) – the first of its kind.” (2010, 447). He shares his discussion in the early 2000’s with Kerr: “I told him [Kerr] of a simple apparatus I had constructed forty years earlier to make two roll-outs: one was of the Fenton Vase, and the other, a fine one from Altar de Sacrificios; he told me he’d seen a copy of the latter, and had been mystified about its origin until that very day.” (Graham 2010, 445–46). Although created in 1966, these rollouts do not seem to appear in any publications prior to 2010. However, with such an early creation date, this rollout photograph by Ian Graham pre-dates both Kerr’s and Imboden’s work by nearly a decade making it the first Maya vase rollout photograph created.

Photogrammetry and Digital Scanning Methods

Photogrammetry has seen widespread adoption, used to create three-dimensional (3D) images from a series of digital still photographs. While this new technique (structure from motion or SfM) has provided an exciting and valuable advancement in artifact archival, limitations exist for current photogrammetry techniques where faithful

photography and color fidelity are critical (Garstki 2017; Felicísimo and Polo 2022). Furthermore, photogrammetry images lose much of their added value when displayed in a two-dimensional (2D) platform such as in print.

A similar documentation method has been explored in recent years for the three-dimensional imaging of artifacts (Tokovinine and Fash 2008). Using three-dimensional scanning equipment, these high resolution images provide a more detailed view of the object, as well as a source for creating 3D-printed replicas (Tokovinine 2013a; Katz and Tokovinine 2017). The capture of high-fidelity three-dimensional images of Maya vases, however, does not address the primary reason for which rollout photography was introduced into this field: the need for a single, flat, contiguous two-dimensional image of the entirety of a vessel's scene, or content. This indicates that three-dimensional imaging is unlikely to replace rollout photography, but will continue in a complementary function, with each technique providing its own distinct contribution towards the study of decorated cylindrical artifacts.

In October 2022, the Los Angeles County Museum of Art (LACMA) published *The Science and Art of Maya Painted Ceramic Vessels*, a freely accessible digital publication, which included newly created digital scanning rollout images for twenty-five cylindrical vessels (Magaloni Kerpel et al. 2022). It provides a unique analysis of these vessels by combining digital rollout photography with infrared and ultraviolet imaging, the first publication of its kind. Interestingly, this modern publication with digitally scanned rollouts specifically mentions Kerr's analog methods, describing them as "early rollouts executed on film" (Magaloni Kerpel et al. 2022, 22).

The digital rollouts created for this 2022 LACMA publication were created using highly specialized scanning equipment, including a 4x5 large format camera, a large format digital scan-back, and a motorized turntable that synchronized its rotation with the camera (Magaloni Kerpel et al. 2022). The cost of this specialized equipment is estimated to be upwards of \$30,000, making this platform generally unattainable for small or local institutions and further hindering the adoption of digital rollout photography. Affordability will be critical to make the transition from “early” rollout methods (film) to the modern digital arena. A low-cost, low-barrier-to-entry platform is needed to promote the adoption of this widespread adoption of this valuable documentation and archival method in a new, digital form.

Making the Case for Rollouts

As mentioned, the usefulness of rollouts, particularly within the realm of Maya vase studies, appears to be generally accepted and not in question. Yet there remains a paucity of discussion specifically addressing the contribution or value of this imaging format in archaeological study. To help fill this gap, I contacted recognized scholars in the field of Maya archaeology to obtain their expert opinions on the importance of having quality rollouts available for study. When these scholars were asked how helpful rollout images are in scholarly study, responses included: “For any comparative analyses it is essential.” (Jennifer Loughmiller-Cardinal, email communication with author, September 1, 2023), and “Visuals are everything, very useful for lectures” (Julie Hoggarth, email communication with author, September 8, 2023). When considered from an art historical, curatorial, or comparative analysis standpoint, this imaging method clearly serves to

enhance the interpretation of both the portrayed scene and the understanding of any text found on the vessel (Magaloni Kerpel et al. 2022).

The Future of Rollouts in the Digital Era

While many publications make note of Justin Kerr's development of his rollout camera and his extensive contribution to the study of Maya art, documentation that details the history of Kerr's rollout development is limited. Additionally, there does not appear to be any literature which discusses the need to bring this valuable documentation method into the digital era, and the benefits of doing so. However, some limited early efforts have been made in recent years to explore the use of digital photography as a source for creating rollouts (Doyle 2016; Felicísimo 2011; Felicísimo et al. 2018).

There is, however, a growing discourse and matching body of literature debating the role that new digital technologies can and should play in the field of archaeology (Daly and Evans 2005; Huggett 2013; 2022; Morgan 2022; Morgan and Eve 2012). Matsumoto (2022, 302) explains the role of digital technology and how many epigraphers see the digitization of epigraphic data as the future of the discipline. By leveraging current advancements in computational photography, combined with archaeological documentation domain knowledge, this project adds to this nascent discussion. Therefore, the point of this thesis is to demonstrate what is currently possible, to examine what limitations currently exist, and to discuss what may be possible in the future based on a robust digital rollout archive.

Chapter III.






Materials and Methodology


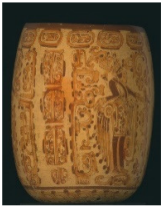




A proof-of-concept experiment was conducted to examine the feasibility of creating archival quality rollout images using a standard, accessible, consumer-priced, and portable digital photography workstation paired with purpose-built software that leverages modern open-source image processing software libraries and commercially available image processing applications. The hardware selected for the source image capture workstation used in these experiments was constructed entirely from commercial off-the-shelf (COTS) components with a target investment goal of under \$4,000. This cost includes the purchase of a standard Canon digital camera which many institutions may already have.

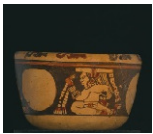



In May of 2023, a selection of fifteen artifacts ($n=15$) from the archives of the Peabody Museum at Harvard University were photographed using custom-developed software, Red Carpet, over a five-day visit. Artifacts were selected to include a variety of vessel sizes, shapes, types, and surfaces in order to evaluate the suitability of rollout automation in various contexts (see Table 1). The images were captured using only this author's equipment, transported in two suitcases from Seattle. The artifacts were photographed at two different locations, which required the setup, teardown, and relocation of the portable workstation. Following the photography sessions, the captured images were processed using Red Carpet to create rollout images from the source digital still photographs. Image processing algorithm experimentation in Red Carpet continued through August of 2023, iteratively improving on and regenerating rollouts to achieve the

final outputs reported on here. These output images were then analyzed and compared against their source images for accuracy, stitching artifacts, and distortion.

Table 1. Artifact selection with difficulty categorization and rationale

R-number	Peabody Museum Identifier	Artifact image*	Rollout Difficulty ---- Rationale
R23003	92-49-20/C182		Simple ---- Minimal curvature with ample surface detail
R23004	35-28-20/4183		Challenge ---- Partial vase reconstruction, minimal surface detail
R23005	09-3-30/75719		Complex ---- Convex and concave curves, ample surface detail
R23006	01-42-20/C3000		Simple ---- Vertical sides, ample surface detail
R23007	37-53-40/3855		Challenge ---- Highly curved, high variations in diameter, protruding handles

R-number	Peabody Museum Identifier	Artifact image*	Rollout Difficulty ---- Rationale
R23008	01-39-20/C2962		Complex ---- Vessel with feet, significant portion of vase has only faint surface detail
R23009	39-8-20/6514		Simple ---- Minimal curvature with ample surface detail
R23010	19-4-20/C9347		Challenge ---- Highly curved with both convex and concave curves
R23011	48-19-20/17785		Simple ---- Vertical sides, uniform color, etched surface
R23012	04-2-20/C3747		Complex ---- Vertical sides, angled base and rim, uniform color, etched surface
R23013	979-14-20/25547		Complex ---- Small (3.6cm diameter), vertical sides, uniform color, etched surface

R-number	Peabody Museum Identifier	Artifact image*	Rollout Difficulty ---- Rationale
R23014	37-129-20/5171		Simple ---- Vertical sides with shallow angle, ample surface detail
R23015	97-44-20/C1855		Complex ---- Vessel with feet, vertical sides, ample surface detail
R23016	39-8-20/6518		Complex ---- Vessel with feet, vertical sides, ample surface detail
R23017	37-129-20/5186		Simple ---- Vertical sides, ample surface detail

**Images by Sandi Reddick from the collection of the Peabody Museum of Archaeology and Ethnology, Harvard University.*

Hardware – The Workstation

Among the goals of this project has been to determine if the current state of digital photography paired with modern image processing algorithms can be leveraged to create a consumer-priced digital rollout workstation, capable of meeting the quality thresholds for academic and artifact archival purposes. For this reason, it was a requirement that all of the equipment used to construct this digital rollout workstation be chosen from publicly available, consumer-grade products. The photography workstation

consisted of a laptop, camera, lenses, tripod light box, two lights, polarization filters, a motorized turntable, and connecting control cables. The camera and lenses were purchased from a local camera equipment store, while the remaining items were purchased directly for home delivery through a major online retailer. Total workstation equipment expenses totaled \$3107, meeting the target goal for a maximum \$4000 budget. See Appendix 2 for the complete list of the workstation components, their procurement sources, and purchase prices.

The Camera Setup

The camera body chosen for use in this project is the Canon EOS R7, a crop frame mirrorless 32.5-megapixel APS-C CMOS sensor camera which retails currently for \$1399. A Canon EOS camera body was chosen for this project as the Canon EOS line of cameras has a freely licensable software development kit which supports software camera control from and image upload to a USB connected computer. The Canon EOS line is also a popular consumer camera model, it is widely available, and the R7 model has one of the higher image resolutions, at 32.5 megapixels. Early in this process development, test images were taken with a Canon EOS Rebel T1i. At a price point of only \$150 for a used camera body, this camera produced good quality images, but with half the resolution at only 15.1 megapixels. Higher image resolutions allow for greater image zoom and larger printing sizes before encountering image deterioration from pixelation. The crop frame format of the R7 model also has a desirable effect for this photography application as the crop factor results in an increased focal length of the lens in use, which in turn extends the depth of field.

A standard 100-400mm focal length telephoto lens was chosen in order to allow photographs to be taken of the imaged artifacts from a distance of approximately 10 feet, using the lens' optical zoom to fill the digital image frame with the target artifact. For this project, the Canon RF100-400mm F5.6-8 IS USM lens was chosen which retails at \$649. Combined with the crop frame image sensor, with a crop factor of 1.6x, this resulted in an increase in the effective focal length range to 160-640mm. The greater depth of field provided by this combination allows for less blurring, essentially imperceptible, along the sides of the curved surfaces of the vessels being photographed, as these sides are marginally further from the camera than the central, primary point of focus.

A good quality tripod is necessary for mounting the camera when taking a series of still images for automated stitching. For this proof-of-concept project, a Manfrotto 3021BN tripod (used, \$135) was obtained. This tripod balanced the weight needed to provide a stable camera platform with the need for portability. A camera battery replacement power adapter was used to eliminate the dependency on battery charges and the possibility of image capture interruption from battery exhaustion (Neewer LP-E6 replacement, retail \$26). In addition, two high speed SDR2/128GB SD cards (Kingston Canvas React Plus 300MB/s, retail \$101/each) were added to the camera so that all of the images captured could remain on camera as backup, in addition to the copy transferred to the laptop during the image capture process. Workstation camera equipment expenses totaled \$2416.

Lighting

Early in the exploration of leveraging software to create digital rollouts, I learned that one of the most important factors to consider in the creation of source digital images

is lighting. Consistent lighting and the elimination of both shadow and glare from the source digital images are paramount to consider when capturing images to be processed with automated stitching or image alignment algorithms. The target artifact must be lit consistently across all of its visible surfaces as well as across the entire set of digital images captured.

To create a controlled and consistent lighting environment for capturing artifact images, a basic 20"x20" light box with black or white colored backdrops was used (Neewer, \$23). The 20" size allowed for artifacts up to approximately 18" tall to be photographed. This size provides enough space to photograph the vast majority of Maya vases and allows adequate height to accommodate the turntable. The purpose of the light box is two-fold. First, it protects against the introduction of unwanted light sources, including reflections, from the surrounding environment. Second, it can provide a consistent backdrop in a solid color for the image background which can be changed as needed, depending on the target vessel to be photographed.

A pair of Switti LED 3000K-8000K light panels were used to provide a consistent source of light. These lights retail for \$284 and come with their own lightweight tripods, travel cases, softboxes for light diffusion (not used in this application), and a remote control. These LED lights were set to 5500K, a standard daylight setting, throughout the image capture process.

When taking photographs, especially with artificial light sources, it is important to manage direct reflection (glare) through the proper placement of those light sources in relation to the camera lens. With a cylindrical target, however, the geometry of a cylinder dictates that there is no position where a light source can be placed that will not result in

direct reflection at the camera lens from the cylinder's surface (Hunter et al. 2015). With no way to eliminate direct reflection through the strategic *positioning* of light sources, an alternative method for eliminating glare on the surface of the target vessels was needed. Polarization of light is a common technique in photography that can be used to address this challenge (Hunter et al. 2015). A polarizing filter was used to convert the light sources into polarized light sources which has the effect of converting direct reflection into polarized reflection. Polarized reflection then can be filtered by adding an appropriately adjusted polarizing filter at the camera lens. To create the polarized light source, a sheet of linear polarizing film (retail \$18) was added to each of the light sources. A circular polarizing filter was also added to the camera (Hoya NXTPlus CIR-PL 67mm, retail \$69) and properly aligned to eliminate glare at the camera lens. Workstation lighting equipment expenses totaled \$394.

Turntable

In order to capture a series of photographs that spans the whole exterior of an object, it is necessary to rotate the object between images. To automate this process, artifacts were placed on top of a remotely controllable turntable (ComXim MT200RUBL20, retail \$110) whose rotation could be controlled via software commands sent over a USB connection. An extended 15' Type A to Type B USB 2.0 cable (\$8) was connected to the turntable and the laptop running the RedCarpet software. Although this turntable is described as having stepper motor-controlled movement at 0.5 and 0.1 degree rotations, the amount of rotation with this turntable is not precise and can drift a little with each movement, causing over or under rotation. This lack of precision was identified

late in the project as it impacted one rollout which will be discussed further in the experiment results. Workstation turntable equipment expenses totaled \$118.

Miscellaneous Hardware

A calibrated color card target is required during post-processing of images to ensure the resulting output images contain accurate color values. This is important data for accuracy in future printing and display. For this project, a Calibrite color card (Calibrite ColorChecker Passport, \$119), card holder (Calibrite ColorChecker Target Holder, \$30), and mounting base (Frienda Tripod Mounting Plate, \$10) were selected to provide a color card that could be stably displayed in proximity to, but without touching, the target artifacts being photographed. For one small artifact, (R23013) a smaller 2"x3" color card was required (CameraTrax, \$20).

The remaining miscellaneous items used as part of the image capture process are items considered to be "on hand" and their costs are not included in the calculation of expenses for this project. This includes the use of a Windows desktop/laptop on which to install and execute the required software. It is expected that this computer is not a dedicated resource, used only for rollout creation, and therefore is not included in the expenses listed to create the rollout workstation. Additional rollout workstation components include power strips, extension cords, gaffer tape, and a tape measure (used for vertical alignment of the artifact, lighting, and camera). Workstation miscellaneous equipment expenses totaled \$179.

Software – Red Carpet

The software used to create the digital rollouts in these experiments was given the name “Red Carpet” by the author, drawing from the well-known phrase “*Roll out the red carpet*”. The core methodology employed to enable the automated creation of digital rollouts (using digital source images and implemented within Red Carpet) was designed and developed by the author. As a software engineer with a background in Computer Vision, I was acutely aware of the multitude of opportunities available to blend my computer science background with my interest in archaeological study. By 2012, I had begun to develop the outline for a method with which digital still images might successfully combine to create digital rollouts entirely in software using basic available image processing and image understanding algorithms.

Background

I first approached Justin Kerr in 2013 at the annual Austin, Texas Maya Meetings to discuss my idea for creating digital rollouts from digital still images. At that time, manual and semi-automated attempts at creating rollouts from digital stills were considered crude and of insufficient quality for use in academic or archaeological documentation purposes. However, after learning that Kodak would discontinue production of the special film he used to make his analog rollouts, Kerr approached me at the 2015 Maya Meetings. At that time, he agreed to provide me with a set of digital photographs at five-degree increments. These digital images were captured at his studio on the same custom-built turntable he had used to create his analog rollouts. Upon receiving those digital images, the development of Red Carpet began with a goal of

creating high-quality, automated digital rollouts using software that leans heavily on principles from computer vision and available image processing methods.

Early feature matching and image stitching attempts quickly revealed that the digital photographs taken by Kerr and sent to me were not ideal for use with digital image processing algorithms. Shadows were present within the images, including shadows which moved on the surface of a vessel from one image to the next. Shadows which move along a vessel's surface during rotation would not be of concern using Kerr's slit-scan analog image capture method, provided the shadows do not appear on the central apex of the vessel. This is due to the fact that the slit-scan method only captures imagery from an extremely narrow view of the object as the object rotates in sync with the movement of the film.

With digital still images, these shadows created significant problems for automated feature detection and correlation between neighboring image pairs. Correlation matching algorithms depend on input images which contain overlapping imagery. This area of overlap is what is used by software algorithms to automatically extract prominent features (feature detection), to match those features between images (correlation matching), and to align and merge the individual images into a rollout (image stitching).

A detailed analysis of the automated feature point detection and correlation mapping in these early failed rollout attempts revealed the problem. When shadows appear in slightly different orientations on a vessel's surface between neighboring images, the relatively prominent contrast changes found along the edges of those shadows create high value points of interest within the images. These strong points of interest were offset between neighboring images as the shadow moved across the vessel

surface. This prevented the correlation matching algorithms from correctly determining the proper image alignment between images, ultimately resulting in significant image stitching and distortion errors.

I have been in co-development with my spouse, Gregory Reddick, since 2015 to produce purpose-built software that supports both digital image capture of, and automated rollout creation from a series of digital still images. Red Carpet is currently a beta quality application that incorporates the author's novel digital image capture and pre-processing algorithms within my partner's custom developed software interface. It integrates and implements these algorithms with third party libraries, open-source packages, and a commercially available panorama stitching utility to achieve successful rollout creation automation. The rollout automation method proposed by this author, and implemented within Red Carpet, is exercised in this proof-of-concept experiment. The goal of this experiment is to evaluate whether or not archival quality digital rollouts can be created from digital still images in a highly automated way, pairing off the shelf hardware with custom-developed, purpose-built image processing software.

Image Capture

Red Carpet automates camera settings and camera operations including shutter control and image upload, using Canon's standard and freely licensable camera control library. Camera settings, including F-stop and ISO are automatically pushed to the camera, but can be manually overridden through the software or directly at the camera. This software also communicates the appropriate turntable control commands via a USB serial port and triggers the desired vessel rotation between photographs.

In preparation for image capture, Red Carpet provides a live camera view of the vessel on the computer with a visual targeting overlay to assist in aligning and centering the vessel on the turntable. The image capture interface can be configured to produce 360 images at one-degree rotations, 180 images at two-degree rotations, or a variety of other image-count/rotation combinations. The software supports capture of two important reference, a color calibration card and a photographic reference scale. In conjunction with image capture, automatic color card detection and color value extraction, for use in color correction, is executed using OpenCV's MCC (Macbeth Chart detector), an open-source C++ computer vision library. This C++ library is accessed via a Python interface. Validation of successful color card capture, detection, and color value extraction are key checkpoints in the image capture process. Extracted color card data is necessary to perform histogram equalization during the image pre-processing phase to achieve proper color balance in the final rollout output images. When the 360-degree image capture process is launched, no interaction with the vessel or equipment is required.

Image Pre-Processing

The image pre-processing algorithms implemented with Red Carpet were developed to enable the highest quality image stitching when using digital still images as inputs. At a high level, Red Carpet implements the following process to prepare a set of digital still images for use in rollout construction:

- Hot pixels and dead pixels, a product of digital camera image sensor flaws, are removed from the images and a median filter is applied to repair any faulty pixels.

- Color correction is applied to each source image based on the color values found in the detected color card.
- The position of the target object and its diameter (in pixels) is determined automatically within the image.
- The optimum vertical image slice width is calculated. This measurement ensures the correct amount of overlap exists between neighboring slices in order to facilitate reliable feature correlation detection and stitching.
- A set of vertical image slices is extracted from the source images.

Rollout Construction

Red Carpet makes use of PTGui, a commercially available panorama stitching utility, with computationally derived inputs, to construct a peripheral photograph from a set of pre-processed digital image slices. The following high-level process is implemented to automatically construct a digital vessel rollout from a set of digital still images:

- Quality bars, alternating black and white lines added to the top and bottom of each image slice, provide additional anchoring correlation points to guide the panorama stitching utility's feature correlation matching process.
- Image slices are forwarded to the panorama stitching utility along with operational settings and computed image orientation data to order and alignment to direct how slices are combined to form a single output image.

- Quality bars are removed, optional image information is added to the image border, and final digital rollout output files are generated in a selection of formats including TIFF and PNG (full size and thumbnail).

Proof of Concept

Fifteen artifacts were chosen from the Harvard Peabody Collection ($n=15$). Object selection was initially limited by their availability during the week of May 11-15, 2023. Most of the objects selected were Maya in origin and cylindrical shaped with straight vertical sides. The selected artifacts were decorated with imagery ideal for presentation in a rollout image and could be considered useful in future study. All artifacts have a Peabody Museum identifier, and each was assigned a unique Red Carpet, or “R” number. This project identifier number is assigned to the imaging project by the software. “R” numbers are constructed from the last two digits of the year the object was photographed, followed by a sequential number indicating the object in the year. Both the Peabody identification number as well as the R number were maintained throughout the imaging process for integrity of the artifact referencing. For the remainder of this thesis, objects and rollouts will be referred to throughout this project by their R number for simplicity and clarity.

For the purposes of this study, objects were initially classified by their form into one of three rollout difficulty categories: *simple*, *complex*, and *challenge*. Vertical cylinders with flat bottoms, little to no curvature, and distinct imagery on the surface to support feature correlation matching were classified in the simple category ($n=6$). Vessels with feet, more highly curved sides, or primarily uniform surface color were classified as complex ($n=6$). Challenge pieces were also selected in order to explore the capability

boundaries of digital image stitching ($n=3$). Challenge pieces included one vessel ($n=1$) with complex curves, one vessel ($n=1$) with complex curves and protruding handles, and one vessel ($n=1$) with minimal surface detail. The complex shapes and limited features found on these vessels make finding common feature points more challenging, which increases the likelihood of improper image alignment and stitching errors in their rollout images.

Process Overview

The automated creation of digital rollouts was accomplished in three distinct phases and all three phases were processed using Red Carpet software. The initial phase prioritized the actual photography, the second phase specifically focused on source image pre-processing, and the third phase generated the rollout.

The image capture phase required a suitable workspace in which to set up the rollout photography workstation and the selected artifacts to photograph. The rollout photography workstation setup diagram is provided in Figure 4. The specific goal of this phase was the capture of high-quality 360-degree digital images and all data necessary for subsequent experiments with automatic rollout creation. It should be noted that once a set of digital images has been captured, image pre-processing and rollout construction phases can be executed entirely independently of the image capture phase. Additionally, these computational phases can also be re-executed multiple times against the same set of source images to achieve different rollout outcomes as different processing options are selected or, over time, as software-implemented algorithms continue to improve. In this experiment, only the digital image capture process was completed at Harvard's Peabody

Museum. The remaining automated image pre-processing and rollout generation was completed later.

Phase One: Image Capture

Phase one was completed over a five-day period in May 2023 in the artifact viewing rooms at Harvard's Peabody Museum and the Peabody Museum Annex. Equipment setup was completed in the artifact viewing room and took approximately 45 minutes. Requirements for the space included providing two sturdy tables on which to place the laptop and turntable, the ability to turn off and/or block out any environmental light, and the availability of power. The turntable and camera were initially positioned about ten feet apart. However, this distance was adjusted based on the size and shape of the artifact to achieve maximum zoom and fill the image frame. The turntable was placed inside the softbox, and lights were positioned close to the object while remaining out of frame.

With the target artifact centered on the turntable by a Peabody staff member, lights and camera were each adjusted to be centered on the same horizontal plane as the vertical center of the target artifact using a standard measuring tape (a laser level could be used here to make the process both quicker and more accurate). Centering and alignment are important factors that must be accounted for to minimize inter-image skew, critical for generating the high-quality input images necessary to achieve successful automated digital rollout creation.

With the target vessel, camera, and lighting properly aligned (with all other room lighting turned off), a polarizing filter on the camera lens was rotated to eliminate direct reflection, or glare, from the surface of the vessel. Color correction card and scale marker

reference images were captured before launching the 360 degree image capture process. The 360 degree image capture process is fully automated by Red Carpet. The software commands the camera shutter release to capture a single image and uploads the image to the connected computer. The software then instructs the turntable to advance its rotation by one degree. Image capture, including project setup, vessel positioning, camera and light position adjustments, reference card image captures, and 360 image capture took approximately 2 hours to complete per vessel. Following completion of the full 360-degree image capture sequence, visual reviews of the images must be done to ensure proper focus and lighting across the set of captured images.

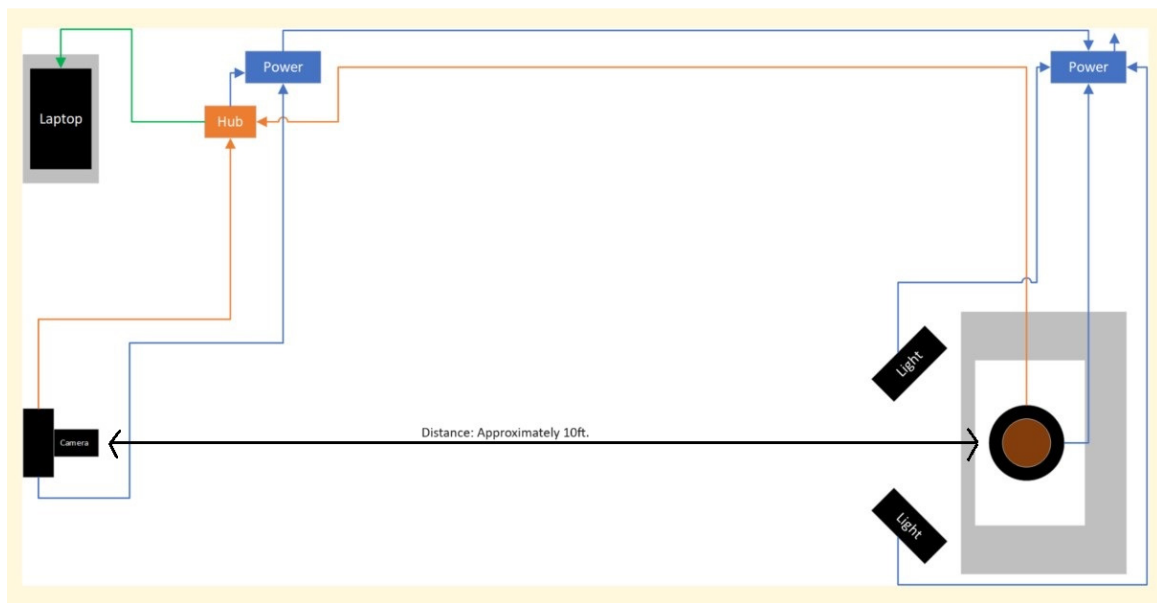


Figure 4. Workstation Setup.

The camera is set up at a distance of approximately ten feet from the target artifact and uses a long focal length lens to achieve a longer focal length. This assists with both flattening of and focus across the entire curved surface of the vessel.

Phase Two: Image Pre-processing

Following the successful capture of images for an object, automated image pre-processing is needed to prepare the digital input images for automated stitching. In order to retain all the original details as captured by the camera, RAW format images are used. RAW format images are uncompressed and unprocessed data, as recorded by the camera's image sensor array. When working with RAW format images, faulty pixels may appear as either black or intensely brightly dots within the RAW images. In digital photography, it is not uncommon for cameras to have a few scattered faulty pixels, especially in cameras with sensors numbering in the millions of pixels. Faulty pixels do not render a digital camera inoperable, and most manufacturers automatically detect and mitigate their impact in the non-RAW image formats they support (e.g. JPEG).

Problematic pixels in the camera's image sensor array may be referred to as dead pixels (those which do not respond to light) or hot pixels (those which are oversensitive to light). The camera used in this project captures images at a resolution of 32 million pixels, commonly referred to as a 32MP or 32 megapixel camera. Of these 32 million pixels, twenty-eight were identified and classified as faulty pixels. In some cases, single faulty pixels were observed causing bleed over into and affecting the color values recorded in adjacent pixels. Each faulty pixel coordinate was given a score between one and three based on how much bleed-over into adjacent pixels was observed. To address the identified hot pixels, I created a spreadsheet of the faulty pixel X,Y coordinates and each of their corresponding bleed-over scores. This data was then provided as a static input to the software. While auto-detection of a camera's faulty pixels would be a desirable feature, it was considered out of scope for the purpose of this project.

Faulty pixels, although nearly imperceptible to the human eye without employing digital zoom, are problematic for image stitching. Feature scanning and matching algorithms detect these faulty pixels and classify them as points of interest for image correlation. Since the position of a hot or dead pixel within an image does not change across the sequence of images as an object is rotated, these aberrant pixels inject faulty feature matching coordinates to the stitching process. To facilitate accurate feature matching across image sequences, hot and dead pixels must be identified and repaired during the image pre-processing phase. An algorithm was developed to read the camera's faulty pixel coordinates and generate a faulty pixel image mask. This mask ensures that pixel repairs can only modify pixels deemed as hot pixels or their color distorted neighbors. This mask was applied to each input image during pre-processing and the faulty pixels were purged then repaired. Hot pixel repair is achieved by calculating estimated correct pixel data, based on the actual correct pixel data available from unaffected neighboring pixels. The affected pixels are set to the estimated correct color values and then a blending algorithm is applied for smoothing within the repaired area. Due to the camera's high resolution at 32MP, these individual pixel level repairs are virtually imperceptible, even when zooming in the view to the individual pixel level.

After correcting faulty pixels in each of the source images, the reference color card was automatically located within the color card image and the 24 color values from the card were extracted. This extracted color data was then compared against the calibrated and known colors for the color card. Color correction offsets along with RGB intercept and slope parameters were automatically calculated and adjustments applied to the input images to correct for color skew which can be introduced by both camera and

lighting. Color correction in photography is frequently performed as manual, subjective post-processing task by the photographer. However, in a lighting controlled environment as defined and implemented in this project, color correction can be performed effectively and automatically within the software using a known reference color card.

With color correction applied, the set of 360 images were first used to generate an animated GIF of the artifact. This animated GIF provides a complementary image to accompany the rollout and provides a rotating view of the imaged vessel resembling a movie. Next a series of image processing algorithms were executed to automatically locate the target object using the first image in the series. With a properly centered vessel, the location of the vessel in the image determined from the first image should be consistent for all images and does not require computation for each image. The method followed to locate the target artifact boundaries includes binary image thresholding, identification of connected components, and bounding box calculations. Identified object boundaries were then used to determine object location, height, and diameter, measured in pixels, within the image. These boundaries were then used to automatically extract relevant image “slices” from the set of source input images.

Although 360 images are captured in one degree increments for each artifact, in general, only sixty images are used for generating the image slices used as inputs to the stitching utility. These image slices are augmented to add features to improve the accuracy of adjoining image feature matching and image stitching. Phase two, image pre-processing, occurred between May 11, 2023, and August 31, 2023, as pre-processing algorithms were executed, evaluated, and re-executed as Red Carpet code was updated to incorporate image processing improvements.

Phase Three: Rollout Creation

Using color corrected and feature augmented image slices and target object size and location as inputs, computationally derived parameters were generated and forwarded to the panorama stitching software. From the composite image, features that were added to facilitate accurate stitching during pre-processing were removed. Final rollout images were generated between August 28, 2023, and September 1, 2023. Final images include a generated image border with artifact identification information along with embedded data that identifies the software version and image creation timestamp within the image's metadata.

Chapter IV

Results and Analysis

This proof-of-concept experiment evaluated automatically generated rollout images across two measures: 1) Are the resulting rollout images “successful” (to be defined later) image constructions? 2) Are the resulting rollout images accurate in the representation of their source artifacts? Both subjective (visual) and objective (automated) scoring methods were employed to evaluate the quality of digital rollouts generated automatically in this experiment. Rollout image result analysis was completed between September 1, 2023, and November 30, 2023. Rollout images are provided in Appendix 1.

Quality Scoring Methodology

For the first measure, a successful rollout is defined as one which correctly combines the distinct digital input images into a visually appealing and reasonably accurate two-dimensional representation of the surface of the original artifact, absent any significant distortions or image stitching errors. Digital imaging applications which create images intended for humans to view continue to be primarily evaluated subjectively by human review (Wang et al. 2004). For this reason, rollout images were first evaluated using manual visual review, looking for the presence of *distortion*, *ghosting*, and *shear*. Distortion is defined as undesirable deformities in the composite image resulting primarily from the projection of a curved surface onto a flat image plane. Ghosting manifests as duplicate, semi-transparent, or missing image elements which may appear in the final composite image where corresponding features from different images fail to be

matched correctly and become duplicated, blended, or overlaid in the final image. Shear appears when straight lines or other object borders fail to align properly where image pairs are joined. Each rollout image was assigned three subjective quality scores for visually observable distortion, ghosting, and shear. Scores assigned ranged from four (excellent/none) to one (significant/extensive). Table 2 provides details on the evaluation criteria used for subjective quality scoring.

Table 2. Subjective Quality Scoring

Score	Distortion	Ghosting	Shear
4 - Excellent	None	None	None
3 - Good	Minimal and necessary for three to two- dimensional transformation	Minimal, trivial, obvious and non-impactful echo ghosting	<10 and non- impactful to artifact imagery
2 - Poor	Significant	Non-trivial but limited	<15 and minimally impactful to artifact imagery
1 - Unacceptable	Extensive/Unacceptable	Extensive ghosting loss	Extensive (>15) or impactful to key artifact imagery

While many of the artifacts chosen for inclusion in this experiment are cylindrical, it is important to recognize that even the most well-formed of these objects are only “roughly” cylindrical and that variations in surface curvature exist across these unique handmade artifacts. It is therefore unavoidable that some amount of distortion will necessarily be introduced when any such variably curved three dimensional surface is projected onto a flat two dimensional plane. To be considered a “successful” projection, distortions must be minimized and limited to only those necessary to achieve a three-dimensional to two-dimensional translation. Additionally, any remaining distortion should result in an image whose differences in detail are essentially indistinguishable from those details when compared with the source. While minor necessary distortions may appear, ghosting and shear should not be apparent in the final images in order to be considered successful.

A second measure, to evaluate the *quality* of the rollout construction process, is an objective method for measuring image correctness. In computer vision and image processing, the Structural Similarity Index Measure (SSIM) excels in performance compared to alternative methods and has proven highly consistent with subjective human assessments of image quality (Li and Bovik 2010). Additionally, SSIM provides a robust automated method with which to evaluate and compare the performance of image stitching algorithms (Boutellier, Tico, and Korhonen 2008).

SSIM scores were generated for each source slice used as input to the rollout stitching process. A median SSIM score for each rollout is derived from these individual slice SSIM scores. The median SSIM score is combined and weighted with the three subjective scores to derive a composite quality score for each rollout.

Subjective Scoring Results

Subjective evaluations, based on manual visual reviews, were completed for all fifteen ($n=15$) artifacts photographed in this project. Occurrences of distortion, ghosting, and shear were identified, and the results of these visual reviews are presented in Table 3.

Distortion

Of the fifteen artifacts photographed, two ($n=2$) included obvious distortion in the final rollout results, R23007 and R23010. Both of these objects have significant diameter variations across their surfaces, and they were both selected as “challenge” objects for this experiment specifically to explore the limits of image stitching when presented with complex curvature. Where significant variations in diameter exist at the source object, stretching and/or compression of the three-dimensional surface to a two-dimensional representation is inevitable. This is not a problem unique to digital imaging and can be compared to the distortion that occurs using Mercator projection of a globe onto a two-dimensional map. In the case of these two objects, however, the two-dimensional projection from automated image feature correlation and stitching resulted in inconsistently distorted features with visually unappealing and unrepresentative changes, when compared to their original images (see Figure 5 and Figure 8). The remaining thirteen ($n=13$) of the fifteen artifacts suffered no obvious distortions during their three-dimensional to two-dimensional translations.

In the case of the complex curvature found in R23007, automated processing based on a single point vessel circumference calculation proved insufficient to guide the three-dimensional to two-dimensional transformation needed to achieve a satisfactory projection. Additional algorithm development to analyze the source artifact’s complex

circumference and surface curvature profile should be explored. It is possible that by providing additional surface slope or curvature analysis as inputs to guide the preprocessing and/or stitching processes, an improved rollout outcome may be achieved.



Figure 5. R23007 distortion example.

Distortion resulting from a highly curved surface. Original source image of curved vessel on left. Distorted two-dimensional projection of figure from automated rollout image on right.

Ghosting

Ghosting was the most frequently occurring image stitching error, appearing one or more times in more than half ($n=8$) of the selected artifacts' rollouts. Ghosting may appear as an echo of small image sections, overlaid and repeated within the final image when they should have been identified within their respective source images as a match and presented once as a single feature in the final rollout. In this discussion, I will refer to this type of ghosting as *echo ghosting*. Ghosting may also present as a loss of image features where source image features failed to align properly and components from one source image overlay, or cover up, other features. I will refer to this type of ghosting as

lost feature ghosting. In this project, the majority of ghosting instances took the form of echo ghosting. This phenomenon involves subtle duplication of features, which is not immediately noticeable when viewing the entire rollout but becomes apparent upon close examination with image zoom. Importantly, this duplication generally does not detract from the overall appearance of the rollout image result.



Figure 6. R23003 ghosting example.

The original source image of the vessel on the left is provided for reference. The middle image close-up shows the original image with details highlighted, while the image on the right shows the ghosting present in the final rollout, a repeated presentation of features due to failure to match them correctly between images.

Echo ghosting manifestations were predominantly noted in regions characterized by prominently sloped vertical surfaces, particularly along the curved bases of vessels such as those found on R23003 and R23009 (See Figure 6 and Figure 7). Although echo

ghosting occurred along the bottom rounded edge on R23009, these errors were scored as non-trivial as they occurred in locations on the vessel that contained painted detail which was altered/duplicated in the final rollout. Both significant echo ghosting and ghosting loss were present in R23010. Here instances of image stitching errors were confined to the profoundly convex curvature observed in the lower region of the vessel, where the slope of the vessel's surface exceeded approximately thirty degrees from vertical (See Figure 8). Of the remaining images where ghosting was observed (R2013, R2014, R2016, and R2017), only minimal non-feature-impacting echo ghosting was present.

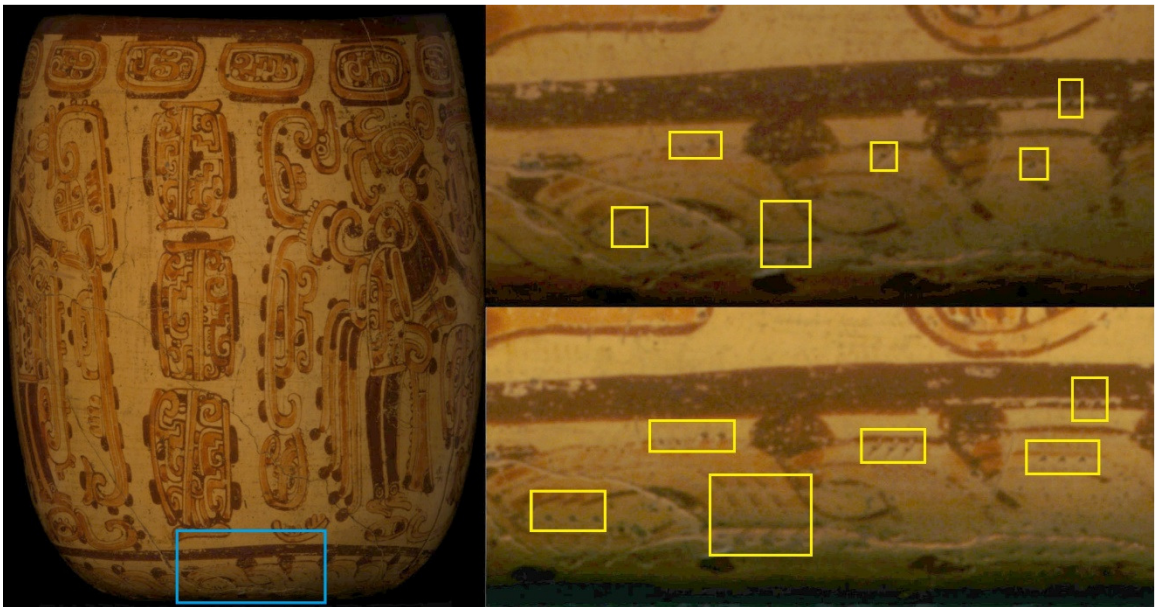


Figure 7. R23009 ghosting example.

The original source image of the vessel on the left is provided for reference. On the right, the top image close-up shows the original image with details highlighted, while the image on the bottom shows the ghosting present in the final rollout. Ghosting like this appeared on vessels where the slope of the vessel exceeded approximately thirty degrees from vertical.

It should be noted that for R23003, R23009, and R23010, echo ghosting appeared only in areas where the slope of the vessel's surface exceeded approximately thirty

degrees from vertical. It is likewise important to acknowledge that at locations where a vertical slope of thirty degrees or more manifests, notably along the curved contours or bases of a vessel, the measured circumference experiences a comparatively rapid alteration. In instances of accelerated changes in vessel circumference, the translation from three-dimensional to two-dimensional representations in adjacent image slices results in heightened feature overlap within the slices corresponding to the more constricted segments of the vessel.

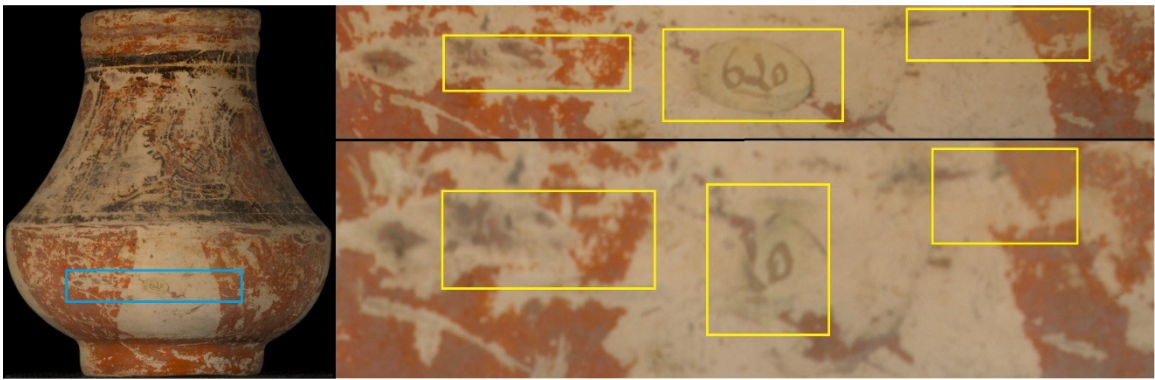


Figure 8. R23010 distortion, ghosting, and shear example.

The original source image of the vessel on the left is provided for reference. On the right, the top image close-up shows the original image with details highlighted, while the image on the bottom shows the ghosting loss and shear present in the final rollout. Significant vertical and horizontal distortion is present in this highly convex vessel base.

Lacking curvature analysis and pre-processing procedures to account for circumference variations in non-cylindrical vessels, the current stitching algorithm exhibits shortcomings. It inadvertently duplicates image segments for spatial fill, leading to image distortion through stretching, thereby introducing echo ghosting. Conversely, during compression, features are overwritten and lost, resulting in ghosting loss as sections of the image undergo undesired reduction. While an analog/film rollout would

not exhibit ghosting when presented with such contours, it would be subject to the same distortions required for three-dimensional to two-dimensional translation.

Shear

Shear is a form of image stitching error which manifests as a discontinuity where lines or feature edges, present within the source images, fail to align properly during the image stitching process resulting in a jagged or non-continuous line in the final image. In five ($n=5$) of the fifteen rollouts (R23003, R23007, R23010, R23014, and R23017), between nine and eighteen instances of shear were observed. R23007 contained the most occurrences of shear at eighteen. These occurrences were evaluated as highly impactful since the misalignments significantly alter the imagery from its original form as viewed on the vessel (see Figure 9). Nine instances of shear were identified on R23003; however, all were present in the highly curved base and considered non-impactful to the final rollout image.

Although R23014 was identified as “simple” in rollout difficulty, the inward slope of the vessel, over twenty percent wider at the top than at its base, proved more of a challenge for the stitching processes than anticipated. Seventeen instances of shear were present, the second highest amount of shear present across all of the rollouts. All of the instances of shear in R23014 occurred within the upper half of the final rollout image (See Figure 10). This suggests software issues with negotiating feature matching in canonical or tapered cylinders, where neighboring/consecutive image pairs consistently contain less overlap in one part of the image slice, in this case the upper half, than they do in other parts of the image slices, such as in the smaller circumference lower half.

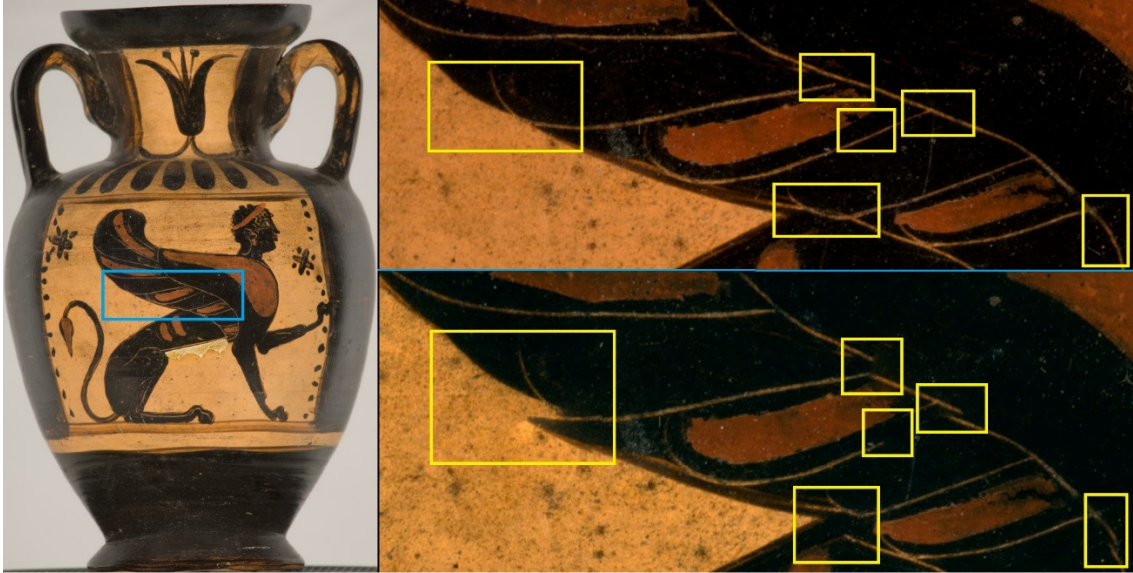


Figure 9. R23007 shear example.

The original source image of the vessel on the left is provided for reference. On the right, the top image close-up shows the original image with details highlighted, while the image on the bottom shows the shear present in the final rollout.

As with the distortion encountered with R23007 due to variations in vessel diameter, additional algorithm development should be explored to analyze the slope of a bowl shaped vessel, or tapered cylinder such as R23007, to support additional automated pre-processing on the source image slices. It is possible that pre-processing, focused on vessel shape analysis in order to enable the creation of image slices with more consistent overlap as inputs to the stitching process, may help to achieve rollout results absent of, or with only minimal, shear on this type of tapered cylinder shaped artifact.

Table 3 lists the subjective scores assigned for each vessel based on manual visual review, along with the average of the subjective scores. In this project, averaged subjective scores ranged between 1.33 and 4.0. R23007 was scored as the least successful rollout at 1.33, while eight ($n=8$) of the fifteen rollouts scored a 4.0 average across the

three subjective measures. This average score was then weighted by the objective score in order to provide a final composite score indicating artifact rollout image quality.



Figure 10.R23014 shear example.

The original source image of the vessel on the top is provided for reference. On the bottom, the left image close-up shows the original image with details highlighted, while the image on the right shows the shear present in the final rollout.

Table 3. Subjective evaluation scores

Vessel	Distortion (D)	Ghosting (G)	Shear (S)	Average (A) $=((D+G+S)/3)$	Scoring Notes
R23003	4	3	3	3.33	Non-impactful ghosting and shear along highly curved bottom edge
R23004	4	4	4	4.0	
R23005	4	4	4	4.0	
R23006	4	4	4	4.0	
R23007	1	2	1	1.33	Significant and obvious distortions throughout. Ghosting and dozens of instances of shear observed.
R23008	4	4	4	4.0	
R23009	4	2	4	3.33	Impactful ghosting along highly curved bottom edge
R23010	3	1	2	2.0	Significant ghosting and shear along highly curved lower half of object
R23011	4	4	4	4.0	
R23012	4	4	4	4.0	
R23013	4	3	4	3.67	Non-impactful ghosting present within the negative spaces of the carving.
R23014	4	3	2	3.0	Ghosting and shear present along upper half of sloped bowl
R23015	4	4	4	4.0	
R23016	4	4	4	4.0	
R23017	4	3	2	3.0	Ghosting and shear present in several areas of detail

Objective Scoring Review

A Structural Similarity (SSIM) Index, first developed by Wang, Bovik, Sheikh, and Simoncelli, was used to evaluate the images generated in this project (2004). This method measures how accurately the details from the original source image slices are reflected within the composite rollout images. SSIM was developed as a way to perform an objective computation-based assessment of an image to predict its perceived image quality (Wang et al. 2004).

In general, Mean Squared Error (MSE) is a widely used algorithm for pixel-by-pixel image quality comparisons, primarily due to its computational simplicity. MSE is referred to as a full-reference quality assessment approach and it is useful in cases where the target output image is expected to exactly match an undistorted reference image. However, MSE depends upon the availability of an original reference image to use for its comparison. Here, no such complete two dimensional reference image exists prior to rollout creation, making MSE unsuitable for this evaluation.

SSIM provides an algorithmically driven evaluation method with which to identify the presence of image feature variations and quantify their impact on perceived image similarity between two corresponding images. It takes into consideration how the human visual system responds to alterations in brightness, contrast, and structure (Wang et al. 2004). This makes it a valuable measure for evaluating image quality in a manner that mirrors human perception.

SSIM analyzes small windows of configurable pixel dimensions between two images and generates a score for them based on brightness, contrast, and features (structure). It repeats this small window comparison across the entirety of the image pair

and generates an overall mean SSIM score, ranging between 0 and 1. The more similar two input images are, the closer the SSIM algorithm's output score is to 1. SSIM also creates a similarity heatmap, an array of local similarity scores, viewable as a grayscale image. In the similarity heatmap image, white indicates similarity while gray and black indicate where distortion or other structural differences were identified between the pair of images being evaluated. The darkest areas indicate locations of greatest dissimilarity between the two images being compared.

For each source image slice provided as input to rollout generation, the location of the input slice's "best matching slice" from the resulting rollout image output was needed. Rollout slices were extracted from within an appropriate target window, or section, of the rollout image, and the best matching rollout slice was determined based on SSIM scoring. In this project, rollout images were constructed using between forty-five and sixty digital source image slices. Therefore, for a rollout, a set of forty-five to sixty SSIM scores is generated with one SSIM score generated for each of that rollout's input image slices. From this set of SSIM scores, the mean of the SSIM values computed across all image slice pairs (source slice and matching rollout slice) is computed. This objective and computationally derived score is used as the final SSIM, or structural similarity, score for the associated rollout.

MATLAB code was developed to execute the best match location and SSIM scoring between the source input slices and resulting output rollout images. MATLAB was chosen due to the robust availability of image processing packages and multiple SSIM image comparison implementations. Based on the Structural Similarity Index algorithm proposed by Wang et al.(2004), the code implemented in this project used an

improved version of the SSIM module implemented for MATLAB. This improved module is called SSIM_INDEX and was developed by Adam Turcotte and Nicolas Robidoux of Laurentian University (2011). All MATLAB code used to perform SSIM scoring is provided in Appendix 3.

Table 4. Structural Similarity (SSIM) Score

Vessel	360 degree Slice Count	SSIM Scores			
		Maximum	Minimum	Average	Median
R23003	52	0.990431	0.970131	0.980474	0.981324
R23004	60	0.998343	0.996767	0.997834	0.997976
R23005	60	0.996556	0.991326	0.994768	0.994945
R23006	60	0.998115	0.943483	0.994685	0.995903
R23007	45	0.946225	0.859383	0.905380	0.898457
R23008	60	0.994537	0.969873	0.986963	0.989173
R23009	60	0.987558	0.972625	0.982774	0.982951
R23010	60	0.977765	0.960241	0.968481	0.968088
R23011	60	0.998473	0.996754	0.997872	0.997916
R23012	60	0.986901	0.970719	0.982779	0.983770
R23013	60	0.974828	0.960661	0.967269	0.966382
R23014	57	0.965667	0.904695	0.936026	0.937450
R23015	59	0.990854	0.982156	0.986815	0.987196
R23016	60	0.996177	0.991147	0.993801	0.993419
R23017	60	0.973923	0.961903	0.967098	0.966957

SSIM scores computed for each artifact.

Structural Similarity (SSIM) scores were computed for each of the fifteen artifacts using MATLAB and the combined results (for all image slice comparisons) are provided in Table 4. SSIM scores for all vessels and all slices are included in Appendix 4. Best matching slice and worst matching slice scores, for R23006 and R23007 respectively, are highlighted in bold within Table 4. R23006 achieved an outstanding median SSIM score of 0.995903 with a maximum (best-match) score of 0.998115. Visual similarity between

the two source images is readily apparent and the mostly white SSIM heatmap provides visual confirmation of this success (see Figure 11).

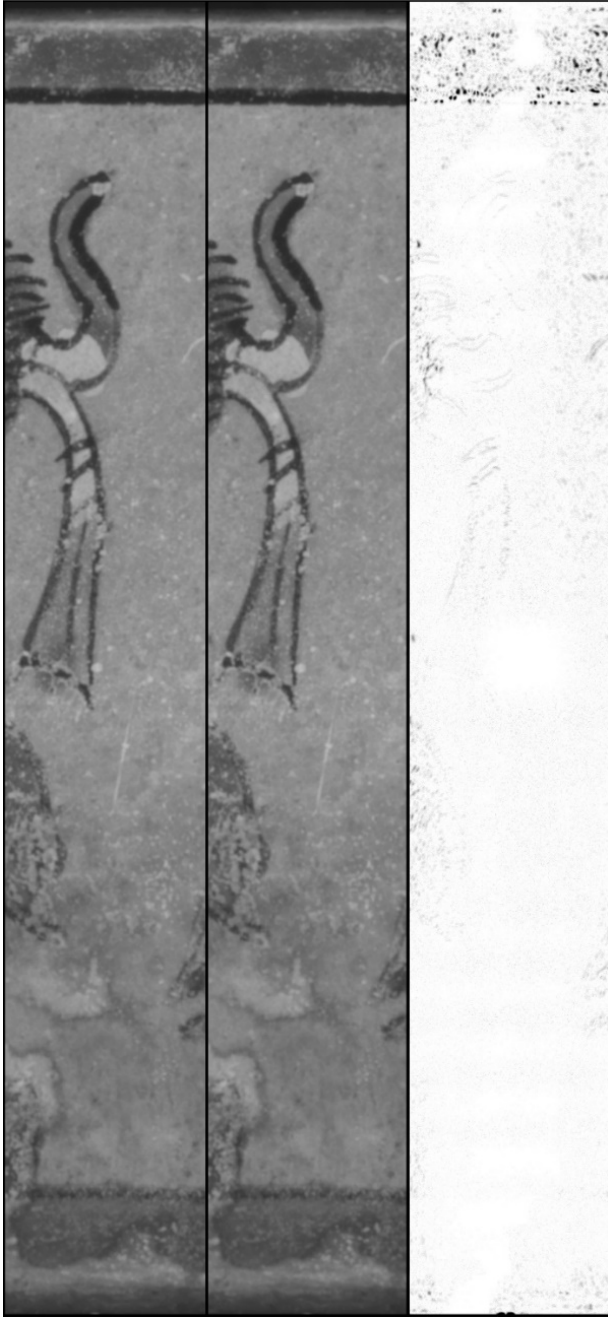


Figure 11.R23006 SSIM maximum (excellent match) example.

Two image slices and SSIM heatmap from an excellent rollout. The source image slice (left), and the rollout image slice (center) were used as inputs for SSIM comparison. The SSIM output heatmap for this image slice pair (right) has a relatively high 0.998115 similarity score.

On the opposite end of the quality spectrum, R23007 had a low mean SSIM score of 0.898457 with a minimum (worst match) score of 0.859383. The image distortion, ghosting, and shear present in R23007 not only resulted in a relatively lower SSIM score, it is also readily apparent in its SSIM heatmaps (see Figure 12).



Figure 12. R23007 SSIM minimum (poor match) example.

Two image slices and heatmap from a poor quality rollout. The source image slice (left), and the rollout image slice (center) were used as inputs for SSIM comparison. The SSIM output heatmap (right) has a relatively low 0.859383 similarity score.

It must be emphasized that SSIM scores are relative measures and do not signify a percentage of correct or incorrect image data. Furthermore, it is essential to recognize that even a suboptimal match may contain a substantial volume of pseudo-matching feature data distributed throughout the image. Regions characterized by blank or solid colored areas, while not constituting an exact match, may contain local similarity within a confined evaluation window. Local window similarity results in elevated SSIM scores and manifests as white areas in the SSIM heatmap image (see Figure 12).

Combined Scoring and Review

Subjective and objective scores were combined to provide a single composite quality score for each rollout. The subjective review score average was weighted using the objective scores from SSIM. Both individual and composite scores for each artifact rollout are provided in Table 5. Rollouts achieving a composite score in the 3.0 to 4.0 range are considered highly successful, excellent quality rollouts. The observation that eleven out of the fifteen rollouts in this study fall within this favorable scoring range is encouraging. This scoring range included rollouts from six vessels initially categorized as “complex”. Additionally, the rollout for one extensively reconstructed vessel, selected as a “challenge” piece due to its limited surface detail over large portions of the vessel, also achieved an overall score in this highest range.








Among the remaining four artifacts, R23014 and R23017 achieved scores between 2.8 and 3.0. These are considered successful rollouts of acceptable quality. It is noteworthy that only two artifacts out of the fifteen chosen yielded unsatisfactory results. These two vessels identified as “challenge” pieces - R23007 and R23010 – attained

composite scores below 2.0. These low scores are attributable to the relatively extensive distortion, ghosting, and shear errors present in their rollouts.

When reviewing R23009, it should be noted that the rollout is incomplete. The edges of this rollout do not match up with one another and a small portion of the vessel, a width of approximately ten degrees, is missing from the final rollout. This was not discovered until later during the image processing phase. While generating an animated GIF for this vessel, it was observed that the 360 images captured for R23009 did not record all 360-degrees of the surface of the vessel. The rotation of the vessel in the animated GIF appeared to jump ahead when viewed in a loop. Visual review confirmed the gap in coverage. While the turntable is not considered a high precision turntable, the speculation here is that during the image capture session, the vessel may have been prone to minute slippage during turntable movements. As this is not a failure of the stitching process, the subjective and objective scores were not reduced based on this lack of 360-degree coverage in the final rollout. An additional process should be added in the image capture phase to ensure full rotational coverage of the vessel at image capture time. Of the fifteen vessels ($n=15$) in this experiment, only one ($n=1$) exhibited this extreme rotational variance during image capture.

Table 5. Artifact distortion, ghosting, shear, and SSIM evaluation results

R-number	Rollout image *see full-page rollout images in Appendix 1	Objective Structural Similarity (SSIM)	Subjective Score Average (A)	SSIM Weighted Composite Score (A*SSIM)
R23003 Excellent		0.981324	3.33	3.2711
R23004 Excellent		0.997976	4.0	3.9919
R23005 Excellent		0.99494	4.0	3.9798
R23006 Excellent		0.995903	4.0	3.9836
R23007 Unacceptable		0.898457	1.33	1.1979
R23008 Excellent		0.989173	4.0	3.9567
R23009 Excellent		0.982951	3.33	3.2765
R23010 Unacceptable		0.968088	2.0	1.9362

R-number	Rollout image *see full-page rollout images in Appendix 1	Objective Structural Similarity (SSIM)	Subjective Score Average (A)	SSIM Weighted Composite Score (A*SSIM)
R23011 Excellent		0.997916	4.0	3.9917
R23012 Excellent		0.983770	4.0	3.9351
R23013 Excellent		0.966382	3.67	3.5434
R23014 Good		0.937450	3.0	2.8124
R23015 Excellent		0.987196	4.0	3.9488
R23016 Excellent		0.993419	4.0	3.9737
R23017 Good		0.966957	3.0	2.9009

**Images by Sandi Reddick from the collection of the Peabody Museum of Archaeology and Ethnology, Harvard University.*

Chapter V.

Conclusions

This investigation sought to ascertain the viability of automatically generated digital rollouts in achieving a level of fidelity suitable for academic scrutiny. This inquiry also aimed to assess the potential of these digital rollouts as a novel standard for the archival documentation of artifacts. The results reported in this thesis have confirmed that it is possible to create highly successful software-generated rollout images, using a low-cost digital photography workstation and purpose-built software that leverages basic image processing and image understanding algorithms. The results have also shown that the automatic creation of rollouts can be achieved with a high level of accuracy across multiple vessel forms and across multiple artifact types. These results have demonstrated sufficient fidelity and measurable quality to support the automated creation of digital rollouts as a viable standard method for artifact archival documentation.

Limitations

To expose the limitations of this technology, the intentional selection of irregular or curvy surfaced artifacts featuring significantly varying circumferences highlighted areas where more attention and development is required. Recognizing that the current software-implemented algorithms contained no support for the evaluation of complex vertical curvature, the flawed results for vessels with these profile characteristics were unsurprising. No attempt was made in the pre-processing or image stitching phases to

address the impacts of circumference variations and no rectifications were applied when creating the input images slices. Additionally, no adjustments were computed for the translation and orientation parameters forwarded to the stitching utility to account for variations in the vessel's surface slope. As a consequence, ghosting and shear appear as common stitching errors on vessels with significantly varying diameters. It is interesting to note that the ghosting errors and shear appeared mainly in predictable locations on these types of surfaces, which may help guide areas for additional focus in future pre-processing algorithm development.

Despite the current limitations, scholars have previously demonstrated that to support certain examinations, even a poorly constructed rollout is preferable to no rollout (Robicsek 1981). Even the least successful rollout examples from this study's results could provide value, with accompanying notes regarding their inaccuracies, to support specific discussions adequately.

Next Steps

Given the findings of this initial work, there are a number of areas that require further consideration. This would include additional algorithm development to identify and analyze a source artifact's curvature profile in the source images should be explored. Artifact surface profile data such as slope can be automatically extracted from the source images. Alternatively, a low cost infrared sensor (e.g. Intel RealSense device) could be incorporated into the workstation to collect detailed depth map data for an artifact at image capture time. Recognizing image zones with significant changes in the vessel's diameter, especially in locations where the slope surpasses a thirty-degree deviation from the vertical, presents an opportunity for informed intervention. Implementing focused

pre-processing strategies to guide the transformation from three-dimensional to two-dimensional in these identified areas shows potential for enhancing the accuracy of feature matching. Consequently, additional pre-processing may reduce or entirely eliminate distortions, ghosting artifacts, and shear effects prevalent in these regions. This has the potential to enable high quality rollout automation for a wider range of complexly shaped artifacts.

The ability to iteratively improve on rollout creation over time may be seen as one of the primary benefits to creating a high-resolution digital source image archive upon which future digital rollouts might be generated. Similarly, as image processing and computational image understanding algorithms advance, the same archive of digital source images might be leveraged for entirely new purposes. As automated digital rollout creation algorithms continue to improve, establishment of a comprehensive digital archive database to capture the necessary inputs to feed this process should begin. The availability of digital images which encompass 360-degrees of an artifact, especially at one degree increments, would provide a solid research base on which rollout development, and other forms of archaeological analysis algorithms, can be built. Future methods, yet to be developed, might include algorithms which can automatically extract and even classify imagery or elements of text from these digital sources.

Appendix 1.

Rollout images

R23003 – Peabody Museum Identifier 92-49-20/C182



*Image by Sandi Reddick from the collection of the Peabody Museum of Archaeology and Ethnology, Harvard University.

R23004 – Peabody Museum Identifier 35-28-20/4183



**Image by Sandi Reddick from the collection of the Peabody Museum of Archaeology and Ethnology, Harvard University.*

R23005 – Peabody Museum Identifier 09-3-30/75719



R23005 09-3-30/75719

© 2023

**Image by Sandi Reddick from the collection of the Peabody Museum of Archaeology and Ethnology, Harvard University.*

R23006 – Peabody Museum Identifier 01-42-20/C3000



**Image by Sandi Reddick from the collection of the Peabody Museum of Archaeology and Ethnology, Harvard University.*

R23007 – Peabody Museum Identifier 37-53-40/3855



**Image by Sandi Reddick from the collection of the Peabody Museum of Archaeology and Ethnology, Harvard University.*

R23008 – Peabody Museum Identifier 01-39-20/C2962



**Image by Sandi Reddick from the collection of the Peabody Museum of Archaeology and Ethnology, Harvard University.*

R23009 – Peabody Museum Identifier 39-8-20/6514



**Image by Sandi Reddick from the collection of the Peabody Museum of Archaeology and Ethnology, Harvard University.*

R23010 – Peabody Museum Identifier 19-4-20/C9347



**Image by Sandi Reddick from the collection of the Peabody Museum of Archaeology and Ethnology, Harvard University.*

R23011 – Peabody Museum Identifier 48-19-20/17785



**Image by Sandi Reddick from the collection of the Peabody Museum of Archaeology and Ethnology, Harvard University.*

R23012 – Peabody Museum Identifier 04-2-20/C3747



**Image by Sandi Reddick from the collection of the Peabody Museum of Archaeology and Ethnology, Harvard University.*

R23013 – Peabody Museum Identifier 979-14-20/25547



**Image by Sandi Reddick from the collection of the Peabody Museum of Archaeology and Ethnology, Harvard University.*

R23014 – Peabody Museum Identifier 37-129-20/5171



**Image by Sandi Reddick from the collection of the Peabody Museum of Archaeology and Ethnology, Harvard University.*

R23015 – Peabody Museum Identifier 97-44-20/C1855



**Image by Sandi Reddick from the collection of the Peabody Museum of Archaeology and Ethnology, Harvard University.*

R23016 – Peabody Museum Identifier 39-8-20/6518



**Image by Sandi Reddick from the collection of the Peabody Museum of Archaeology and Ethnology, Harvard University.*

R23017 – Peabody Museum Identifier 37-129-20/5186



**Image by Sandi Reddick from the collection of the Peabody Museum of Archaeology and Ethnology, Harvard University.*

Appendix 2.

Rollout Workstation Components, Costs, and Sources

Table 6. Workstation Hardware

Component	Make/Model	Purchase Price	Source w/Link
Digital camera body	Canon EOS R7, Mirrorless, 32.5MP	\$1399	Local camera store. Available via Amazon.com
SD Memory Cards	2 - Kingston Canvas React Plus 128GB SDXC USH-II 300R/260W U3 V90	\$202	Amazon.com
USB Camera Cable (Laptop to Camera)	USB 2.0 to Mini-B USB Cable, 6.5 ft	\$5	Amazon.com
Camera Power Adapter	Neewer LP-E6 battery replacement	\$26	Amazon.com
Telephoto lens	Canon RF100-400mm F5.6-8	\$649	Local camera store. Available via Amazon.com
Tripod	Manfrotto 3021BN (pre-owned)	\$135	Local camera store. Available via NTC-Tech
Light box	Neewer 20"x20" Square Light Box with four backgrounds	\$23	Amazon.com. Discontinued. Similar item available via Amazon.com
Light panels w/stands	Switti LED Light Panel Kit, 3000-8000K	\$284	Amazon.com
Polarizing Filter	Hoya 67mm NXT CIR-PL	\$69	Local camera store. Available via Amazon.com
Polarizing Film	Renianus 20x30cm Polarized Film Sheets	\$18	Amazon.com
Software Controllable Turntable	ComXim MT200RUWL20 7.87" USB Turntable	\$110	Amazon.com. Currently available from AliExpress
USB Printer Cable (Laptop to Turntable)	Nanxudyj 15ft USB 2.0 Printer Cable	\$8	Amazon.com

Component	Make/Model	Purchase Price	Source w/Link
Color card	Calibrite ColorChecker Passport 2	\$119	Amazon.com
Color card stand	Calibrite ColorChecker Holder	\$30	Amazon.com
Color card stand base	Frienda Tripod Mounting Plate	\$10	Amazon.com
Small color card	CameraTrax 2x3 24 Color Card	\$20	Amazon.com

Appendix 3.

MATLAB Code Used in Objective Quality Analysis

SSIM_INDEX.m

```
function [mssim, ssim_map] = ssim_index(img1, img2 , K, window, L)
%=====
%Edited code by Adam Turcotte and Nicolas Robidoux
%Laurentian University
%Sudbury, ON, Canada
%Last Modified: 2011-01-22
%-----
%This code implements a refactored computation of SSIM that requires
%one fewer blur (4 instead of 5), the same number of pixel-by-pixel
%binary operations (10), and two fewer unary operations (6 instead of 8).
%As a result, it is about 20% faster.
%In addition, this version reduces memory usage with in-place functions.
%As a result, it supports larger input images.
%=====
%=====
%SSIM Index, Version 1.0
%Copyright(c) 2003 Zhou Wang
%All Rights Reserved.
%
%The author is with Howard Hughes Medical Institute, and Laboratory
%for Computational Vision at Center for Neural Science and Courant
%Institute of Mathematical Sciences, New York University.
%
%-----
%Permission to use, copy, or modify this software and its documentation
%for educational and research purposes only and without fee is hereby
%granted, provided that this copyright notice and the original authors'
%names appear on all copies and supporting documentation. This program
%shall not be used, rewritten, or adapted as the basis of a commercial
%software or hardware product without first obtaining permission of the
%authors. The authors make no representations about the suitability of
%this software for any purpose. It is provided "as is" without express
%or implied warranty.
%-----
%
%This is an implementation of the algorithm for calculating the
%Structural SIMilarity (SSIM) index between two images. Please refer
%to the following paper:
%
%Z. Wang, A. C. Bovik, H. R. Sheikh, and E. P. Simoncelli, "Image
%quality assessment: From error measurement to structural similarity"
%IEEE Transactions on Image Processing, vol. 13, no. 1, Jan. 2004.
```

```

%
%Kindly report any suggestions or corrections to zhouwang@ieee.org
%-----
%
%Input : (1) img1: the first image being compared
%         (2) img2: the second image being compared
%         (3) K: constants in the SSIM index formula (see the above
%             reference). default value: K = [0.01 0.03]
%         (4) window: local window for statistics (see the above
%             reference). default window is Gaussian given by
%             window = fspecial('gaussian', 11, 1.5);
%         (5) L: dynamic range of the images. default: L = 255
%Output: (1) mssim: the mean SSIM index value between 2 images.
%           If one of the images being compared is regarded as
%           perfect quality, then mssim can be considered as the
%           quality measure of the other image.
%           If img1 = img2, then mssim = 1.
%           (2) ssim_map: the SSIM index map of the test image. The map
%           has a smaller size than the input images. The actual size:
%           size(img1) - size(window) + 1.
%
%Default Usage:
%   Given 2 test images img1 and img2, whose dynamic range is 0-255
%
%   [mssim ssim_map] = ssim_index(img1, img2);
%
%Advanced Usage:
%   User defined parameters. For example
%   K = [0.05 0.05];
%   window = ones(8);
%   L = 100;
%   [mssim ssim_map] = ssim_index(img1, img2, K, window, L);
%
%See the results:
%   mssim %Gives the mssim value
%   imshow(max(0, ssim_map).^4) %Shows the SSIM index map
%
%=====
if (nargin < 2 || nargin > 5)
    ssim_index = -Inf;
    ssim_map = -Inf;
    return;
end

if (size(img1) ~= size(img2))
    ssim_index = -Inf;
    ssim_map = -Inf;
    return;
end

[M N] = size(img1);

if (nargin == 2)
    if ((M < 11) || (N < 11))
        ssim_index = -Inf;
    end
end

```

```

        ssim_map = -Inf;
        return
    end
    window = fspecial('gaussian', 11, 1.5);    %
    K(1) = 0.01;                               % default settings
    K(2) = 0.03;                               %
    L = 65535;                                 %
end

if (nargin == 3)
    if ((M < 11) || (N < 11))
        ssim_index = -Inf;
        ssim_map = -Inf;
        return
    end
    window = fspecial('gaussian', 11, 1.5);
    L = 255;
    if (length(K) == 2)
        if (K(1) < 0 || K(2) < 0)
            ssim_index = -Inf;
            ssim_map = -Inf;
            return;
        end
    else
        ssim_index = -Inf;
        ssim_map = -Inf;
        return;
    end
end

if (nargin == 4)
    [H W] = size(window);
    if ((H*W) < 4 || (H > M) || (W > N))
        ssim_index = -Inf;
        ssim_map = -Inf;
        return
    end
    L = 65535;
    if (length(K) == 2)
        if (K(1) < 0 || K(2) < 0)
            ssim_index = -Inf;
            ssim_map = -Inf;
            return;
        end
    else
        ssim_index = -Inf;
        ssim_map = -Inf;
        return;
    end
end

if (nargin == 5)
    [H W] = size(window);
    if ((H*W) < 4 || (H > M) || (W > N))
        ssim_index = -Inf;

```

```

        ssim_map = -Inf;
    return
end
if (length(K) == 2)
    if (K(1) < 0 || K(2) < 0)
        ssim_index = -Inf;
        ssim_map = -Inf;
        return;
    end
else
    ssim_index = -Inf;
    ssim_map = -Inf;
    return;
end
end
end

C1 = (K(1)*L)^2;
C2 = (K(2)*L)^2;
window = window/sum(sum(window));
img1 = double(img1);
img2 = double(img2);

ssim_map = filter2(window, img1, 'valid'); % gx
w1 = filter2(window, img2, 'valid'); % gy
w2 = ssim_map.*w1; % gx*gy
w2 = 2*w2+C1; % 2*(gx*gy)+C1 = num1
w1 = (w1-ssim_map).^2+w2; % (gy-gx)^2+num1 = den1
ssim_map = filter2(window, img1.*img2, 'valid'); % g(x*y)
ssim_map = (2*ssim_map+(C1+C2))-w2; % 2*g(x*y)+(C1+C2)-num1 =
num2
ssim_map = ssim_map.*w2; % num
img1 = img1.^2; % x^2
img2 = img2.^2; % y^2
img1 = img1+img2; % x^2+y^2

if (C1 > 0 && C2 > 0)
    w2 = filter2(window, img1, 'valid'); % g(x^2+y^2)
    w2 = w2-w1+(C1+C2); % den2
    w2 = w2.*w1; % den
    ssim_map = ssim_map./w2; % num/den = ssim
else
    w3 = filter2(window, img1, 'valid'); % g(x^2+y^2)
    w3 = w3-w1+(C1+C2); % den2
    w4 = ones(size(w1));
    index = (w1.*w3 > 0);
    w4(index) = (ssim_map(index))./(w1(index).*w3(index));
    index = (w1 ~= 0) & (w3 == 0);
    w4(index) = w2(index)./w1(index);
    ssim_map = w4;
end
end

mssim = mean2(ssim_map);

return

```

SSIM_ROLLOUT_TEST_DRIVER.m

```
%=====
%SSIM Rollout Test Driver, Version 1.0
%Code by Sandra Reddick
%Harvard University
%Cambridge, MA, USA
%Last Modified: 2023-11-18
%-----
%This code evaluates the structural similarity between source image
%slices and Red Carpet rollout image results. It computes the Structural
%Similarity Index (SSIM)score between two images based on the
%following paper:
%
%Z. Wang, A. C. Bovik, H. R. Sheikh, and E. P. Simoncelli, "Image
%quality assessment: From error measurement to structural similarity"
%IEEE Transactions on Image Processing, vol. 13, no. 1, Jan. 2004.
%
%This code leverages the improved SSIM_INDEX module, developed by Adam
%Turcotte and Nicolas Robidoux of Laurentian University.
%-----
%Permission to use, copy, or modify this software and its documentation
%for educational and research purposes only and without fee is hereby
%granted, provided that this copyright notice and the original authors'
%names appear on all copies and supporting documentation. This program
%shall not be used, rewritten, or adapted as the basis of a commercial
%software or hardware product without first obtaining permission of the
%authors. The authors make no representations about the suitability of
%this software for any purpose. It is provided "as is" without express
%or implied warranty.
%=====
% create a pool of parallel processes for faster slice processing
parpool('Processes');

%=====
%===== BEGIN Modifiable parameters =====
```

```

%=====
% SSIM constant, defaults for rollout analysis: K = [0.002, 0.03]
K = [0.002, 0.03];
% image comparison window
% small gaussian window and sigma used to reduce smoothing
window = fspecial('gaussian', 3, 0.3);
% scan window size to look for "best match" in rollout image
mssim_window = 200;
% quality bar height added to top/bottom of Red Carpet source slice images
qualityBarHeight = 55;
% + or - value to adjust best match location scan. Needed due to
% Red Carpet non-precision vessel image capture rotation variance.
rotationalVarianceAdjust = 0;
% root directory for all vessel image data
rootDir = 'D:\Vessels';
% Name of Red Carpet vessel directory to process
% Must be located directly under rootDir
Vessel = 'R23017#01';
% Location to write shared output results Excel file
matlabDir = 'D:\Matlab';
% Comparison image output directory. Must be under vessel directory.
testDir = 'Test';
% Source image input directory. Must be under vessel directory
processDir = 'Process';
%=====
%==== END Modifiable parameters =====
%=====

projectFilePath = fullfile(rootDir,Vessel);
testFilePath = fullfile(projectFilePath,testDir);
processFilePath = fullfile(projectFilePath,processDir);
rolloutFilename = fullfile(processFilePath,'Rollout-Raw.tif');
SliceFileNames = dir(fullfile(processFilePath,'Slice*.tif'));
SlicesCount = length(SliceFileNames);
% Get raw rollout image
rgbRollout = imread(rolloutFilename);

```

```

% Remove transparency layer - SSIM doesn't support it
rgbRollout = rgbRollout(:,:,1:3);
grayRollout = rgb2gray(rgbRollout);
[grayRolloutHeight,grayRolloutWidth] = size(grayRollout);
% Remove quality bars from the full raw rollout image
grayRollout = imcrop(grayRollout,[0 qualityBarHeight grayRolloutWidth (grayRolloutHeight-(qualityBarHeight*2))]);
% Get new rollout image size with quality bars removed
[grayRolloutHeight,grayRolloutWidth] = size(grayRollout);
% Optional for troubleshooting - Write out grayscale rollout img
%imwrite(grayRollout,fullfile(testFilesPath,'grayRollout.tiff'));

% Initialize the mssim_array - 2D float output array
mssim_array = zeros(SlicesCount,mssim_window+1);
for iParam=1 : 1 : SlicesCount
    rgbSliceFile = imread(fullfile(processFilesPath, strcat('Slice',num2str(iParam,'%04.f'),'.tif')));
    % Remove transparency layer - SSIM doesn't support it
    rgbSliceFile = rgbSliceFile(:,:,1:3);
    graySlice = rgb2gray(rgbSliceFile);
    [graySliceHeight,graySliceWidth] = size(graySlice);
    % Remove quality bars from the slice image
    graySlice = imcrop(graySlice,[0 qualityBarHeight graySliceWidth (graySliceHeight-(qualityBarHeight*2))]);
    % Get new Slice image size with quality bars removed
    [newSliceHeight,newSliceWidth] = size(graySlice);
    % Resize slice to rollout height - Comparison image sizes MUST match
    imgSlice = imresize(graySlice,[grayRolloutHeight NaN],Antialiasing=false);
    imwrite(imgSlice,fullfile(testFilesPath, strcat('Slice',num2str(iParam,'%04.f'),'_Source.tif')));
    [imgSliceHeight, imgSliceWidth] = size(imgSlice);
    % Determine leftmost X position to start extracting rollout slices
    % Guestimates best match location with rotational variance adjustment
    rolloutXstart = min((((grayRolloutWidth/(SlicesCount+2)) * (iParam-1)) + (rotationalVarianceAdjust * (iParam-1))),grayRolloutWidth - imgSliceWidth);

    scan_window = mssim_window*2 +1;
    parfor jParam = 1 : 1 : mssim_window + 1
        jOffset = ((jParam - 1) * 2) - mssim_window;

```

```

    if ((rolloutXstart+jOffset >= 0) && (rolloutXstart+jOffset+imgSliceWidth <= grayRolloutWidth) && ((iParam ~= 1)
|| ((iParam == 1) && (jOffset >= 0))) && ((iParam ~= SlicesCount) || ((iParam == SlicesCount) && (jOffset <=0))))
        % Create rollout slice to use for comparison
        rolloutSlice = imcrop(grayRollout, [rolloutXstart+jOffset 0 imgSliceWidth imgSliceHeight]);
        rolloutSlice = imcrop(rolloutSlice, [0 0 imgSliceWidth imgSliceHeight]);
        % Optional for troubleshooting
        % - Write out all rollout slice candidate image

%imwrite(rolloutSlice,fullfile(testFilesPath, strcat('RolloutSlice', num2str(iParam, '%04.f'), '_', num2str(jParam, '%02.
f'), '.tiff')));
        [mssim, ssim_map] = ssim_index(rolloutSlice, imgSlice, K, window, 65535);
        % Optional for troubleshooting
        % - Write out all SSIM result candidate images
        %imwrite(ssim_map,
fullfile(testFilesPath, strcat('SSIM', num2str(iParam, '%04.f'), '_', num2str(jParam, '%02.f'), '.tiff')));
        mssim_array(iParam, jParam) = mssim
    end
end
% Find index of best match in rollout for this input slice
bestMatchIndex = 1;
bestMatchValue = 0.0;
for jParam = 1 : 1 : mssim_window + 1
    if (mssim_array(iParam, jParam) > bestMatchValue)
        bestMatchIndex = jParam;
        bestMatchValue = mssim_array(iParam, jParam);
    end
end
% Using best match index, regenerate images and write to test directory
bestMatchOffset = ((bestMatchIndex - 1) * 2) - mssim_window;
rolloutSlice = imcrop(grayRollout, [rolloutXstart+bestMatchOffset 0 imgSliceWidth imgSliceHeight]);
rolloutSlice = imcrop(rolloutSlice, [0 0 imgSliceWidth imgSliceHeight]);

imwrite(rolloutSlice, fullfile(testFilesPath, strcat('Slice', num2str(iParam, '%04.f'), '_Rollout_', num2str(bestMatchInd
ex, '%02.f'), '.tiff')));
[mssim, ssim_map] = ssim_index(rolloutSlice, imgSlice, K, window, 65535);

```



```

imwrite(ssim_map,fullfile(testFilesPath, strcat('Slice', num2str(iParam, '%04.f'), '_SSIM_', num2str(bestMatchIndex, '%02
.f'), '_Score_', num2str(bestMatchValue, '%.10f'), '.tiff')));
    % Write all SSIM candidate scores for slice to Excel spreadsheet
    SSIMResultsSpreadsheetFilename = fullfile(matlabDir, testDir, 'SSIM_Results.xlsx');
    writematrix(mssim_array, SSIMResultsSpreadsheetFilename, 'Sheet', Vessel, 'Range', 'F2');
end
% clear the parallel processor pool
delete(gcp('nocreate'));

```

Appendix 4.

SSIM Results

Vase R-number	R23003	R23004	R23005	R23006	R23007	R23008	R23009	R23010
MEDIAN	0.981324	0.997953	0.994898	0.995418	0.898457	0.989302	0.982779	0.966699
MAX	0.990431	0.998343	0.996556	0.998115	0.946225	0.994537	0.987834	0.977765
MIN	0.970131	0.996767	0.991326	0.988984	0.859383	0.969873	0.978149	0.960678
AVERAGE	0.980576	0.997796	0.994544	0.994272	0.905090	0.987531	0.982766	0.967775
Source Slice Count	52	60	60	60	45	60	60	60
Individual Slice Scores								
1	0.984410	0.998090	0.995627	0.991943	0.927225	0.993553	0.978750	0.962690
2	0.984889	0.997901	0.994467	0.990458	0.939242	0.989680	0.980898	0.965776
3	0.981961	0.997718	0.992743	0.996055	0.940652	0.988280	0.980542	0.966096
4	0.980973	0.997535	0.991331	0.992881	0.938402	0.990359	0.981941	0.965705
5	0.979194	0.997338	0.992627	0.990134	0.921829	0.990660	0.980320	0.965367
6	0.976710	0.996873	0.993693	0.990544	0.884554	0.990874	0.980867	0.964658
7	0.974375	0.997090	0.992335	0.993575	0.876275	0.988523	0.981344	0.963572
8	0.971769	0.996878	0.991869	0.988984	0.878574	0.988391	0.983462	0.964886
9	0.970646	0.996821	0.991326	0.992819	0.865788	0.989851	0.985361	0.965525
10	0.970771	0.996767	0.992678	0.995950	0.868218	0.992691	0.986239	0.966199
11	0.970784	0.997063	0.995049	0.993426	0.883898	0.987823	0.985246	0.966038
12	0.970786	0.997197	0.994557	0.993201	0.880726	0.990511	0.987834	0.965359
13	0.970893	0.997127	0.994453	0.992781	0.883058	0.992914	0.987228	0.966010

Vase R-number	R23003	R23004	R23005	R23006	R23007	R23008	R23009	R23010
14	0.972827	0.997104	0.995011	0.995608	0.884784	0.989417	0.984270	0.966866
15	0.975801	0.997376	0.995337	0.994977	0.879416	0.991770	0.983441	0.967533
16	0.980738	0.997583	0.995804	0.996810	0.880785	0.990115	0.979942	0.966288
17	0.984020	0.997737	0.995095	0.994385	0.909787	0.990935	0.981056	0.966420
18	0.981768	0.997962	0.995611	0.995399	0.931656	0.985673	0.984000	0.967485
19	0.974504	0.998000	0.995924	0.996701	0.943715	0.981063	0.983644	0.966532
20	0.970131	0.998052	0.994897	0.995099	0.944823	0.984282	0.984804	0.965306
21	0.975294	0.998140	0.995116	0.996544	0.944230	0.981486	0.983218	0.962400
22	0.982162	0.998160	0.994925	0.995488	0.945302	0.980054	0.983258	0.961784
23	0.986321	0.998239	0.994996	0.994020	0.945416	0.984090	0.982574	0.960678
24	0.986335	0.998180	0.995924	0.995093	0.946225	0.989187	0.980946	0.963751
25	0.984337	0.997994	0.994866	0.996262	0.943221	0.992271	0.982010	0.968088
26	0.982459	0.997951	0.994987	0.994515	0.939762	0.990760	0.982692	0.967539
27	0.981279	0.997977	0.995575	0.994216	0.919635	0.989034	0.984158	0.968731
28	0.980342	0.997976	0.995320	0.995134	0.898457	0.990603	0.983310	0.966912
29	0.981837	0.997917	0.995601	0.996703	0.878478	0.991017	0.983281	0.963700
30	0.983103	0.997843	0.995293	0.995903	0.879376	0.989173	0.983079	0.961157
31	0.984679	0.997909	0.994602	0.996778	0.882185	0.989649	0.982500	0.961421
32	0.984929	0.997945	0.994964	0.996030	0.880044	0.986781	0.983117	0.961104
33	0.984437	0.998088	0.994290	0.996729	0.869845	0.989597	0.985751	0.961834
34	0.981690	0.998003	0.994531	0.997534	0.873726	0.982239	0.987558	0.962098
35	0.981369	0.998006	0.993746	0.997634	0.865263	0.983368	0.986965	0.963863
36	0.980863	0.998017	0.992691	0.997296	0.859383	0.988848	0.984909	0.965562
37	0.979169	0.997914	0.993002	0.997387	0.869965	0.986769	0.980156	0.967483
38	0.977340	0.997808	0.993598	0.996301	0.874148	0.987423	0.978149	0.969177
39	0.977646	0.997826	0.993220	0.997468	0.871197	0.983462	0.980864	0.972776
40	0.980846	0.997844	0.993284	0.998115	0.907259	0.981341	0.984185	0.974618

Vase R-number	R23003	R23004	R23005	R23006	R23007	R23008	R23009	R23010
41	0.984962	0.997955	0.994707	0.996135	0.926585	0.976058	0.985978	0.975216
42	0.988489	0.998172	0.995823	0.996996	0.929634	0.969873	0.985037	0.974618
43	0.990390	0.998343	0.994131	0.997680	0.943521	0.972084	0.982337	0.973794
44	0.988185	0.998303	0.994919	0.997077	0.945837	0.975881	0.981753	0.972036
45	0.983441	0.998159	0.995706	0.997116	0.926955	0.980654	0.982866	0.971466
46	0.979606	0.998172	0.994296	0.996164	N/A	0.981429	0.982588	0.971048
47	0.977702	0.998296	0.993900	0.995384	N/A	0.980531	0.983476	0.969820
48	0.979988	0.998115	0.995100	0.995437	N/A	0.985080	0.982584	0.969730
49	0.984074	0.998073	0.995598	0.996740	N/A	0.990218	0.981704	0.969987
50	0.988520	0.997442	0.995415	0.995316	N/A	0.993351	0.981090	0.971122
51	0.990431	0.997264	0.994336	0.995248	N/A	0.990749	0.980090	0.972385
52	0.989771	0.996912	0.994493	0.995227	N/A	0.993218	0.981888	0.973769
53	N/A	0.997305	0.995076	0.996297	N/A	0.990372	0.981920	0.976649
54	N/A	0.997782	0.994617	0.994468	N/A	0.988609	0.980676	0.977765
55	N/A	0.998192	0.994987	0.992962	N/A	0.994340	0.981335	0.977330
56	N/A	0.998274	0.994825	0.995340	N/A	0.991836	0.983036	0.976123
57	N/A	0.998257	0.994899	0.996198	N/A	0.994537	0.985268	0.974442
58	N/A	0.998279	0.996216	0.992899	N/A	0.992810	0.983656	0.971601
59	N/A	0.998234	0.996054	0.993257	N/A	0.991894	0.982167	0.968378
60	N/A	0.998295	0.996556	0.943483	N/A	0.993823	0.972625	0.960241

Vase R-number	R23011	R23012	R23013	R23014	R23015	R23016	R23017
MEDIAN	0.997915	0.981964	0.967056	0.940280	0.986369	0.993203	0.967718
MAX	0.998473	0.986901	0.974828	0.965667	0.990854	0.996177	0.975077
MIN	0.996754	0.966488	0.960661	0.904695	0.980621	0.989925	0.961903
AVERAGE	0.997843	0.980934	0.967578	0.937438	0.986384	0.993525	0.967809
Source Slice Count	60	60	60	57	59	60	60
Individual Slice Scores							
1	0.998363	0.980630	0.968254	0.950208	0.986497	0.995303	0.969299
2	0.998018	0.980207	0.967351	0.951348	0.985140	0.994237	0.974128
3	0.997492	0.979572	0.968225	0.944147	0.984801	0.992996	0.970969
4	0.997680	0.978386	0.967989	0.940280	0.980621	0.993431	0.969521
5	0.997810	0.978334	0.963830	0.936052	0.982115	0.993091	0.970338
6	0.998014	0.978212	0.965065	0.935592	0.984587	0.992199	0.972467
7	0.998079	0.977895	0.965219	0.936230	0.983230	0.991377	0.969849
8	0.998002	0.977689	0.966623	0.932155	0.985807	0.992068	0.968747
9	0.997918	0.977278	0.965582	0.928825	0.988219	0.989925	0.966936
10	0.998052	0.976209	0.965809	0.930619	0.983558	0.991181	0.967020
11	0.997520	0.973165	0.972152	0.935125	0.984950	0.993020	0.964440
12	0.997236	0.970763	0.970789	0.941198	0.985951	0.991282	0.965148
13	0.996870	0.969579	0.971847	0.945591	0.986163	0.992876	0.968095
14	0.997396	0.966488	0.972891	0.949592	0.985191	0.992174	0.968263
15	0.997980	0.966531	0.971374	0.950550	0.986102	0.992499	0.970744
16	0.997990	0.970719	0.971812	0.942350	0.987592	0.993694	0.967435
17	0.998408	0.972033	0.973690	0.943063	0.987916	0.994342	0.966408
18	0.997864	0.977300	0.974828	0.946432	0.988792	0.994323	0.967850
19	0.998013	0.978787	0.974030	0.949814	0.988495	0.995675	0.971900
20	0.998016	0.980643	0.974434	0.944479	0.988746	0.995284	0.975077
21	0.997932	0.983518	0.973980	0.929576	0.988773	0.995677	0.973395

Vase R-number	R23011	R23012	R23013	R23014	R23015	R23016	R23017
22	0.997802	0.982656	0.973824	0.919445	0.989205	0.995834	0.973923
23	0.997920	0.983064	0.973973	0.904695	0.989445	0.996101	0.967874
24	0.997995	0.984113	0.972802	0.905290	0.989386	0.996177	0.968138
25	0.997912	0.985183	0.971569	0.908074	0.990854	0.995879	0.964468
26	0.997947	0.985400	0.971140	0.914680	0.987464	0.995368	0.967158
27	0.998183	0.984663	0.970310	0.918498	0.987196	0.995543	0.966471
28	0.998310	0.983779	0.968706	0.918668	0.986248	0.995646	0.965978
29	0.997647	0.983476	0.966956	0.918618	0.985655	0.994938	0.968072
30	0.997412	0.984321	0.967187	0.923212	0.984428	0.995095	0.966440
31	0.997431	0.983996	0.968343	0.936385	0.985836	0.995383	0.966757
32	0.997544	0.983751	0.965886	0.950065	0.986084	0.995021	0.961903
33	0.997388	0.984244	0.963121	0.946745	0.987782	0.994449	0.967331
34	0.996765	0.984707	0.964686	0.938514	0.988200	0.994043	0.965766
35	0.996754	0.985495	0.966138	0.944957	0.988319	0.993156	0.966296
36	0.997669	0.986123	0.963722	0.949282	0.988844	0.993297	0.964685
37	0.998133	0.986712	0.960661	0.947750	0.987511	0.992522	0.965129
38	0.998123	0.986643	0.964803	0.940870	0.986268	0.993073	0.964907
39	0.998293	0.986566	0.967155	0.931377	0.985181	0.994194	0.963873
40	0.998382	0.986405	0.965796	0.924165	0.986916	0.993174	0.967712
41	0.998288	0.986436	0.966263	0.916546	0.984002	0.992481	0.967550
42	0.998473	0.986901	0.966500	0.920369	0.982526	0.992543	0.964380
43	0.998435	0.985018	0.965383	0.923541	0.984098	0.993571	0.963180
44	0.998351	0.983770	0.965631	0.929991	0.986369	0.993945	0.963592
45	0.998269	0.981659	0.967304	0.928445	0.984445	0.993231	0.966300
46	0.997830	0.980872	0.968407	0.925768	0.986391	0.992036	0.967725
47	0.997403	0.980902	0.967862	0.930700	0.987967	0.992662	0.968957
48	0.997569	0.982491	0.967751	0.943637	0.988447	0.993028	0.969242

Vase R-number	R23011	R23012	R23013	R23014	R23015	R23016	R23017
49	0.998172	0.983837	0.963982	0.951727	0.989569	0.992570	0.967728
50	0.997797	0.985199	0.963278	0.956876	0.988679	0.991881	0.970338
51	0.997716	0.985352	0.963939	0.954205	0.987973	0.993419	0.970215
52	0.997847	0.983811	0.963309	0.953220	0.986753	0.992253	0.969060
53	0.997578	0.982182	0.962394	0.952234	0.988447	0.992503	0.966486
54	0.997409	0.981044	0.962620	0.956954	0.984935	0.992943	0.965221
55	0.997507	0.980910	0.962130	0.962155	0.982997	0.992763	0.965744
56	0.997836	0.981069	0.961827	0.965667	0.985864	0.993681	0.967916
57	0.997801	0.981452	0.962598	0.957405	0.983217	0.991147	0.969354
58	0.997753	0.981746	0.966091	N/A	0.982156	0.992959	0.969746
59	0.997958	0.981626	0.969294	N/A	0.987756	0.992713	0.969789
60	0.998311	0.974501	0.965555	N/A	N/A	0.993652	0.965131

References

- Boutellier, Jani, Marius Tico, and Lassi Korhonen. 2008. "Objective Evaluation of Image Mosaics." In *Computer Vision and Computer Graphics: Theory and Applications*, 107–17. Berlin: Springer-Verlag.
- Coe, Michael D. 1973. *The Maya Scribe and His World*. New York: The Grolier Club.
- . 1975. *Classic Maya Pottery at Dumbarton Oaks*. Washington, DC: Dumbarton Oaks Trustees for Harvard University.
- Coe, Michael D., and Justin Kerr. 1978. *Lords of the Underworld: Masterpieces of Classic Maya Ceramics*. Princeton, NJ: Art Museum, Princeton University.
- Daly, Patrick, and Thomas L Evans. 2005. "Introduction: Archaeological Theory and Digital Pasts." In *Digital Archaeology: Bridging Method and Theory*, 2–7. London: Routledge.
- Doyle, James. "Unrolling the Ceramic Canvases of Maya Painters." *Now at the Met* (blog). November 28, 2016. <https://www.metmuseum.org/blogs/now-at-the-met/2016/unrolling-maya-ceramic-canvases>.
- Fash, William Leonard. 2001. *Scribes, Warriors and Kings: The City of Copán and the Ancient Maya*. Rev. ed. New Aspects of Antiquity. London: Thames & Hudson.
- Felicísimo, Ángel M. 2011. "Vase Rollout Photography Using Digital Reflex Cameras." *Technical Briefs in Historical Archaeology* 6: 28–32.
- Felicísimo, Ángel M., and María-Eugenia Polo. 2022. "Measurement and Control of Colour Fidelity in Scanned 3D Models for Heritage Conservation." *Journal of Cultural Heritage* 56: 159–66.
- Felicísimo, Ángel M., María-Eugenia Polo, Guadalupe Durán-Domínguez, Trinidad Tortosa, and Alicia Rodero. 2018. "Rollout Archaeological Photography for the Graphic Documentation of Cultural Heritage." In *Proceedings of the 23rd International Conference on Cultural Heritage and New Technologies 2018*, edited by Wolfgang Börner and Susanne Uhlirz. Vienna: Museen der Stadt Wien – Stadtarchäologie.
- Garstki, Kevin. 2017. "Virtual Representation: The Production of 3D Digital Artifacts." *Journal of Archaeological Method and Theory* 24 (3): 726–50.
- Graham, Ian. 2010. *The Road to Ruins*. Albuquerque: University of New Mexico Press.

- Hay, Clarence L., Lothrop, Samuel K., Linton, Ralph L., Shapiro, Harry L., and Vaillant, George C., eds. 1940. *The Maya and Their Neighbors*. Limited ed. New York: D. Appleton-Century.
- Huggett, Jeremy. 2013. "Disciplinary Issues: Challenging the Research and Practice of Computer Applications in Archaeology." In *Archaeology in the Digital Era: Papers from the 40th Annual Conference of Computer Applications and Quantitative Methods in Archaeology (CAA), Southampton, 26-29 March 2012*, edited by Graeme Earl, Tim Sly, Angeliki Chrysanthi, Patricia Murrieta-Flores, Constantinos Papadopoulos, Iza Romanowska, and David Wheatley, 13–24. Amsterdam: Amsterdam University Press.
- . 2022. "Data Legacies, Epistemic Anxieties, and Digital Imaginaries in Archaeology." *Digital 2* (2): 267–95.
- Hunter, Fil, Steven Biver, Paul Fuqua, and Robin Reid. 2015. *Light–Science & Magic: An Introduction to Photographic Lighting*. 6th ed. New York: Routledge.
- Katz, Jared, and Alexandre Tokovinine. 2017. "The Past, Now Showing in 3D: An Introduction." *Digital Applications in Archaeology and Cultural Heritage* 6: 1–3.
- Kerr, Barbara, and Justin Kerr. 2005. "The 'Way' of God L: The Princeton Vase Revisited." *Record of the Princeton Art Museum* 64: 71–79.
- Kerr, Justin. "A Short History of Rollout Photography." FAMSI Foundation for the Advancement of Mesoamerican Studies, Inc. November 8, 2007. <http://www.famsi.org/research/kerr/rollout.html>.
- . n.d. "Maya Vase Database: An Archive of Rollout Photographs." Maya Vase Database. <http://www.mayavase.com/>.
- Kerr, Justin, Michael D. Coe, Mary Ellen Miller, and Linda Schele. 1989. *The Maya Vase Book: A Corpus of Rollout Photographs of Maya Vases*. Vol. 1. New York: Kerr Associates.
- Kerr, Justin, Nikolai Grube, Barbara MacLeod, and Brian Stross. 1990. *The Maya Vase Book: A Corpus of Rollout Photographs of Maya Vases*. Vol. 2. New York: Kerr Associates.
- Kerr, Justin, Simon Martin, Inga E. Calvin, Michel Quenon, and Genevieve Le Fort. 1997. *The Maya Vase Book: A Corpus of Rollout Photographs of Maya Vases*. Edited by Barbara Kerr. Vol. 5. New York: Kerr Associates.
- Kerr, Justin, Dorie Reents-Budet, Marc Zender, Carolyn E. Tate, Patricia Ancona-Ha, Jorge Pérez de Lara, and Mark Van Stone. 2000. *The Maya Vase Book: A Corpus of Rollout Photographs of Maya Vases*. Edited by Barbara Kerr. Vol. 6. New York: Kerr Associates.

- Kerr, Justin, Jennifer T. Taschek, Joseph Walter Ball, Stephen D. Houston, David Stuart, Karl A. Taube, and Dicey Taylor. 1992. *The Maya Vase Book: A Corpus of Rollout Photographs of Maya Vases*. Vol. 3. New York: Kerr Associates.
- Kerr, Justin, Karl A. Taube, Nikolai Grube, and Werner Nahm. 1994. *The Maya Vase Book: A Corpus of Rollout Photographs of Maya Vases*. Edited by Barbara Kerr. Vol. 4. New York: Kerr Associates.
- Li, Chaofeng, and Alan C. Bovik. 2010. "Content-Partitioned Structural Similarity Index for Image Quality Assessment." *Signal Processing. Image Communication* 25 (7): 517–26.
- Lockwood, George J., and Andrew Davidhazy. "Looking at Life Through a Slit in the Camera." *Milwaukee Journal Insight*, June 27, 1971.
- Loughmiller-Newman, Jennifer A. 2008. "Canons of Maya Painting: A Spatial Analysis of Classic Period Polychromes." *Ancient Mesoamerica* 19 (1): 29–42.
- Magaloni Kerpel, Diana, Megan E. O'Neil, Oswaldo Fernando Chinchilla Mazariegos, Charlotte Eng, Hector L. Escobedo, John W. Hirx, Stephen D. Houston, et al. 2022. *The Science and Art of Maya Painted Ceramic Vessels: Contextualizing a Collection*. Los Angeles: Los Angeles County Museum of Art.
<https://archive.org/details/maya-painted-ceramic-vessels>.
- Matsumoto, Mallory E. 2022. "Archaeology and Epigraphy in the Digital Era." *Journal of Archaeological Research* 30 (2): 285–320.
- "Maya Polychrome Cylinder Vase Late Classic, Circa AD 550-950." Sotheby's. 2019.
<https://www.sothebys.com/en/buy/auction/2019/art-of-africa-oceania-and-the-americas/maya-polychrome-cylinder-vase-late-classic-circa>.
- Miller, Mary Ellen, and Claudia Brittenham. 2013. *The Spectacle of the Late Maya Court: Reflections on the Murals of Bonampak*. William & Bettye Nowlin Series in Art, History, and Culture of the Western Hemisphere. Austin: University of Texas Press.
- Morgan, Colleen. 2022. "Current Digital Archaeology." *Annual Review of Anthropology* 51 (1): 213–31. <https://doi.org/10.1146/annurev-anthro-041320-114101>.
- Morgan, Colleen, and Stuart Eve. 2012. "DIY and Digital Archaeology: What Are You Doing to Participate?" *World Archaeology* 44 (4): 521–37.
<https://doi.org/10.1080/00438243.2012.741810>.
- Museum of Modern Art [MoMA]. Press release no. 62, June 20, 1967.
https://www.moma.org/documents/moma_press-release_326517.pdf.

- Rands, Robert L. 1974. "The Ceramic Sequence at Palenque, Chiapas." In *Mesoamerican Archaeology: New Approaches*, edited by Norman Hammond. Austin: University of Texas Press.
- Reents-Budet, Dorie. 1994. *Painting the Maya Universe: Royal Ceramics of the Classic Period*. Durham: Duke University Press.
- Robicsek, Francis. 1981. *The Maya Book of the Dead: The Ceramic Codex ; the Corpus of Codex Style Ceramics of the Late Classic Period*. Charlottesville: University of Virginia Art Museum.
- Spinden, Herbert J. 1913. *A Study of Maya Art: Its Subject Matter and Historical Development*. Cambridge, MA: Peabody Museum Press.
- Stone, Andrea Joyce, and Marc Zender. 2011. *Reading Maya Art: A Hieroglyphic Guide to Ancient Maya Painting and Sculpture*. New York: Thames & Hudson.
- Stuart, David. 2011. *The Order of Days: The Maya World and the Truth About 2012*. New York: Harmony Books.
- Stuart, George E. 1975. "Riddle of the Glyphs." *National Geographic*, December 1975.
- Tokovinine, Alexandre. 2013a. "Corpus of Maya Hieroglyphic Inscriptions 3D Imaging Report." https://peabody.harvard.edu/files/scan_report_2013_high_all1y.pdf.
- . 2013b. *Place and Identity in Classic Maya Narratives*. Washington, DC: Dumbarton Oaks Research Library and Collection.
- Tokovinine, Alexandre, and Barbara Fash. 2008. "Scanning History: The Corpus of Maya Hieroglyphic Inscriptions Tests a 3-D Scanner in the Field." *Symbols* (Spring): 17–19.
- Turcotte, Adam, and Nicolas Robidoux. 2011. "SSIM_INDEX." Laurentian University. <http://ssim.rivetsforbreakfast.com/>.
- Wang, Zhou, Alan Conrad Bovik, Hamid Rahim Sheikh, and Eero P. Simoncelli. 2004. "Image Quality Assessment: From Error Visibility to Structural Similarity." *IEEE Transactions on Image Processing* 13 (4): 600–612.